This article has been accepted for publication in a future issue of this journal, but has not been fully edited. Content may change prior to final publication. Citation information: DOI 10.1109/TAC.2021.3124979, IEEE Transactions on Automatic Control

Topology Learning of Linear Dynamical Systems with Latent Nodes using Matrix Decomposition

Mishfad Shaikh Veedu*,[1], *Student Member, IEEE*, Harish Doddi*,[2], and Murti V. Salapaka[1], *Fellow, IEEE*

***Abstract*— In this article, we present a novel approach to reconstruct the topology of networked linear dynamical systems with latent nodes. The network is allowed to have directed loops and bi-directed edges. The main approach relies on the unique decomposition of the inverse of power spectral density matrix (IPSDM) obtained from observed nodes as a sum of sparse and low-rank matrices. We provide conditions and methods for decomposing the IPSDM of the observed nodes into sparse and low-rank components. The sparse component yields the moral graph associated with the observed nodes, and the low-rank component retrieves parents, children and spouses (the Markov Blanket) of the hidden nodes. The article provides necessary and sufficient conditions for the unique decomposition of a given skew symmetric matrix into sum of a sparse skew symmetric and a low-rank skew symmetric matrices. It is shown that for a large class of systems, the unique decomposition of imaginary part of the IPSDM of observed nodes, a skew symmetric matrix, into the sparse and the low-rank components is sufficient to identify the moral graph of the observed nodes as well as the Markov Blanket of latent nodes. For a large class of systems, all spurious links in the moral graph formed by the observed nodes can be identified. Assuming conditions on hidden nodes required for identifiability, links between the hidden and observed nodes can be reconstructed, resulting in the retrieval of the exact topology of the network from the availability of IPSDM. Moreover, for finite number of data samples, we provide concentration bounds on the entry-wise distance between the true IPSDM and the estimated IPSDM.**

I. Introduction

Networks provide convenient representation of large scale complex systems utilized in diverse areas such as power grids, biology, finance, and neuroscience. Reconstructing the underlying network topology or the influence structure of the interaction from measurements is useful in predicting, and steering the behavior of the system towards a desired state. Learning the unknown interaction structure of a network of agents from time-series measurements can be categorized as being active [1] or passive [2]. Active techniques require intervention in the normal operation of the system by injection of external signals and/or altering the network structure, by removing or adding agents to the network. Many critical systems such as the power grid, the financial markets, and the meteorological system either do not allow for active interventions or it is not possible to affect the system. On the contrary, passive techniques infer topology from time-series measurements, without affecting the underlying grid network. Here, in practice, observing time-series measurement at every node is not plausible, wherein it becomes important to learn the topology of the network when only a subset of the nodes are observed.

Learning the topology of a network from time-series data is an active area of research, with considerable emphasis from the machine learning and probabilistic graphical model communities (see [1]-[6]). However, here, most works assume that the nodes are random variables which fail to capture the dynamics of the interaction and thus are improper for the applications with dynamic dependencies that are common, for example, in the power grid [7] and its application to smart grid networks [8], climate science [9] and finance [10]. Moreover, in many scenarios, topology identification is the first step in system identification[11], [12].

Filtering based topology reconstruction has gained considerable attention recently for unveiling the topology of dynamically related agents. In [13], the moral graph of a directed network is reconstructed using the magnitude response of multivariate Wiener filters. [14] provided a method that showed that the spurious links present in the moral graph can be removed by checking the phase response of the Wiener filter between the links. [13] and [15] provided algorithms for exact network reconstruction where all parent-child relations are uncovered but the results are restricted using Granger causality to systems with strictly causal dynamical dependencies. The aforementioned works, [13]-[15], assumed full network observability. Several works, [17]-[22], have studied topology identification in the presence of hidden nodes, but, restricted to radial tree topologies–characterized by undirected tree topology in [17], for polyforest networks in [18], and polytree networks in [19]-[21]. Network reconstruction with corrupted data streams was explored in [25]-[27].

In [29]-[35], the authors considered the problem of estimating conditional dependency structure of autoregressive (AR) Gaussian stochastic processes in the presence of latent nodes, with an emphasis on finiteness of the time-series available. Here, the problem is formulated in terms of sparse plus low-rank decomposition of the inverse of the power spectral density matrix (IPSDM). The articles [29]-[35] provided interesting optimization frameworks and theoretical guarantees to identify the conditional dependency from estimated IPSDM. Here, the graphical representations of conditional dependencies reconstructed from the IPSDM retrieves the moral graph [13]. As shown in [13], [36], moral

[1]Mishfad S. Veedu and Murti V. Salapaka are with Department of Electrical and Computer Engineering, University of Minnesota, Minneapolis, USA, veedu002@umn.edu, murtis@umn.edu

[2]Harish Doddi is with Department of Mechanical Engineering, University of Minnesota, Minneapolis, USA, doddi003@umn.edu

*Mishfad S. Veedu and Harish Doddi contributed equally to this work.
This work was partially supported by NSF and ARPA-E

0018-9286 (c) 2021 IEEE. Personal use is permitted, but republication/redistribution requires IEEE permission. See http://www.ieee.org/publications_standards/publications/rights/index.html for more information.
Authorized licensed use limited to: University of Minnesota. Downloaded on August 12,2022 at 21:08:33 UTC from IEEE Xplore. Restrictions apply.

This article has been accepted for publication in a future issue of this journal, but has not been fully edited. Content may change prior to final publication. Citation information: DOI 10.1109/TAC.2021.3124979, IEEE Transactions on Automatic Control

graphs can admit many spurious edges.

In this article, we approach the problem of reconstructing the topology in the presence of latent nodes. Similar to [29]-[35] a perspective of sparse plus low-rank decomposition of IPSDM associated with the observed nodes is taken.

Extending the results in [37], this article establishes conditions for a skew symmetric to admit a unique decomposition as a sparse and low-rank matrix. Towards decomposing a skew symmetric matrix, this article provides a characterization for tangent manifolds of skew symmetric matrices with a fixed rank and with a given sparsity pattern. Furthermore, the article provides additional theoretical insights into an empirical procedure presented in [37], which provides a sufficient condition that can be tractably assessed for a unique decomposition. Though not emphasized in the article, the methodology developed can be used to realize similar results for unique decomposition of Hermitian matrices as well.

Based on the extensions of the results in [37] established here, it is possible to obtain a decomposition of the IPSDM of the observed nodes, where the sparse part can be leveraged to realize the moral graph formed by the observed nodes. We establish identifiability conditions under which the low-rank component of the observed nodes' IPSDM yields the parents, children and spouses (all the the two hop neighbors that form the Markov Blanket) of the latent (hidden) nodes. The IPSDM, being complex and frequency dependent, has real and imaginary parts. We further emphasize the imaginary part of the IPSDM in the article as it has considerable structure applicable for a large class of problems. Here too the sparse component of the imaginary part of the IPSDM matrix, which is skew symmetric, is shown to yield the moral graph of networks governed by a linear dynamical model (defined later) that encompass a wide class of systems. The above approach can be employed toward the retrieval of the moral graph of networks of AR models and is applicable to networked systems addressed in [29] albeit, here we do not emphasize the finite data aspects.

The moral graph relations can admit many spurious connections not present in the original topology. We demonstrate that the rank-sparsity patterns induced by the network topology on the imaginary part has properties that can be exploited toward the *exact* reconstruction of network topology. Here, under assumptions applicable for a large class of systems, all spurious links in the moral graph formed by observed nodes can be identified. Moreover, assuming conditions on hidden (latent) nodes, which follow from identifiability conditions, links between the hidden and observed nodes can be reconstructed resulting in the retrieval of the exact topology of the network.

This article also serves as an important bridge between the works presented in [37] and the works related to network structure reconstruction [13]-[24]. Furthermore, results here are applicable to many classes of directed graphs without self loops, not restricted to directed acyclic graphs or bi-directed graphs, unlike [14], [17].

We summarize below the major contributions of the article.

- Provides non-trivial generalizations of results of [37] to skew symmetric matrices, with exact characterization of tangent manifolds of skew symmetric matrices with a given rank and skew symmetric sparse matrices. We also provide a sufficient condition that enables a practical way to select penalty factor for the convex optimization formulation that yields the unique, sparse plus low-rank matrix decomposition, restricted to skew symmetric matrices. This contribution is applicable to general skew symmetric matrix independent of its application to topology identification.
- Reconstructs the moral graph of observed nodes and the Markov Blanket of latent nodes from the matrix decomposition of IPSDM; accounting for network identifiability issues associated with the latent nodes.
- Establishes that the decomposition of imaginary part of IPSDM is sufficient to recover moral graph of observed nodes and the Markov Blanket of the latent nodes. Conditions and methods for unique decomposition as a sum of low rank and sparse matrices of the imaginary part are provided.
- For large class of systems, the exact topology of the entire network is reconstructed by the decomposition of imaginary part of the IPSDM.
- For the more practical scenarios where we have access only to finite samples of time-series at each node, we provide a concentration bound for estimation error of IPSDM.

Organization of the article: Section II presents the unique decomposition of a skew symmetric matrix into its sparse and low-rank components. Section III discusses linear dynamical systems and its graphical representation. Section IV addresses moral graph reconstruction, identifiability of latent nodes, and Markov Blanket reconstruction of the latent nodes. Exact topology reconstruction is studied in Section V. Section VI discusses IPSDM estimation from finite time series. Section VII provides simulation results and Section VIII concludes the article.

Notations: Bold capital letters denote matrices and bold small letters denote vectors. $\mathbb{S}^n$ denotes the set of all $n \times n$ skew symmetric matrices with real entries. For a matrix $\mathbf{M}$, $[\mathbf{M}]_{ij}$, $\mathbf{M}_{ij}$, or $\mathbf{M}(i,j)$ denote the (i,j)-th element of $\mathbf{M}$, $\|\mathbf{M}\|_1$ is defined as $\sum_{i,j}|\mathbf{M}_{ij}|$, $\|\mathbf{M}\|_\infty$ is defined as $\max_{ij}|\mathbf{M}_{ij}|$, and $\|\mathbf{M}\|_0$ denotes the number of non-zero entries in $\mathbf{M}$. $\|\mathbf{M}\|_*$ denotes the nuclear norm, which is the sum of singular values of $\mathbf{M}$, and $\|\mathbf{M}\|_2$ denotes spectral-norm, which is defined as the largest singular value. $support(\mathbf{M})$ is defined as $\{(i,j) : \mathbf{M}_{ij} \neq 0\}$. $\Im\{\mathbf{M}\}$ denotes imaginary part of $\mathbf{M}$. For a vector, $\|\mathbf{x}\|_2$ denotes euclidean-norm, defined as $\sqrt{\sum_i x_i^2}$. $\sigma_i(\mathbf{M})$ denotes i^{th} largest singular value of $\mathbf{M}$. For time-series $(\widetilde{x}_i(t))_{t\in\mathbb{Z}}$, $\mathbf{x}(z) = \mathcal{Z}[\widetilde{\mathbf{x}}(k)]$ denotes bilateral z-transform of $\widetilde{\mathbf{x}}$. For a set $\mathcal{S}$, $|\mathcal{S}|$ denotes cardinality of the set. We use $j = \sqrt{-1}$. For a transfer function $h(z), z \in \mathbb{C}$, $h = 0$ means h is identically zero, i.e., $h(z) = 0$ for every $|z| = 1$. $h \neq 0$ means h is not identically zero. Almost always or almost surely is defined for a probability measure

0018-9286 (c) 2021 IEEE. Personal use is permitted, but republication/redistribution requires IEEE permission. See http://www.ieee.org/publications_standards/publications/rights/index.html for more information.
Authorized licensed use limited to: University of Minnesota. Downloaded on August 12,2022 at 21:08:33 UTC from IEEE Xplore. Restrictions apply.

This article has been accepted for publication in a future issue of this journal, but has not been fully edited. Content may change prior to final publication. Citation information: DOI 10.1109/TAC.2021.3124979, IEEE Transactions on Automatic Control

that is absolutely continuous with respect to the Lebesgue measure (e.g. any continuous distribution).

II. Sparse plus Low-Rank Matrix Decomposition for Skew Symmetric Matrices

In this section, we discuss the following problem: suppose we are given a real skew symmetric matrix $\mathbf{C} \in \mathbb{S}^n$ that is obtained by adding a sparse matrix $\tilde{\mathbf{S}} \in \mathbb{S}^n$ and a low-rank matrix $\tilde{\mathbf{L}} \in \mathbb{S}^n$; when can we decompose the matrix and retrieve the component matrices? The material presented in this section provides the needed preliminaries and extensions of results from [37], which do not incorporate constraints of skew symmetry. We remark that the results discussed in this section for the space of skew symmetric matrices can be extended to the space of complex matrices. However, we do not discuss it here.

A. Optimization for Sparse plus Low-rank Decomposition

Consider the following optimization problem.

$$\begin{aligned}(\hat{\mathbf{S}}_{\boldsymbol{\gamma}}, \hat{\mathbf{L}}_{\boldsymbol{\gamma}}) \quad = \quad & \arg\min_{\mathbf{S},\mathbf{L}} \gamma\|\mathbf{S}\|_0 + rank(\mathbf{L}) \\ & \text{subject to } \mathbf{S}+\mathbf{L}=\mathbf{C}, \\ & \qquad \mathbf{S}+\mathbf{S}^T=\mathbf{0},\ \mathbf{L}+\mathbf{L}^T=\mathbf{0},\end{aligned} \tag{1}$$

where γ is a fixed penalty, selected a priori. (1) is a combinatorial optimization problem and is NP-hard [38]. ℓ_1 norm is often employed as a surrogate for ℓ_0 norm [39], with nuclear norm being a proxy for rank [40]. Thus a more tractable convex relaxation associated with (1) is:

$$\begin{aligned}(\hat{\mathbf{S}}_{\boldsymbol{\gamma}}, \hat{\mathbf{L}}_{\boldsymbol{\gamma}}) \quad = \quad & \arg\min_{\mathbf{S},\mathbf{L}} \boldsymbol{\gamma}\|\mathbf{S}\|_1 + \|\mathbf{L}\|_* \\ & \text{subject to } \mathbf{S}+\mathbf{L}=\mathbf{C}, \\ & \qquad \mathbf{S}+\mathbf{S}^T=\mathbf{0},\ \mathbf{L}+\mathbf{L}^T=\mathbf{0}.\end{aligned} \tag{2}$$

Remark 1: Given $\mathbf{C} = -\mathbf{C}^T$, imposing the constraint $\mathbf{S}+\mathbf{S}^T=\mathbf{0}$ renders $\mathbf{L}+\mathbf{L}^T$ superfluous.

In this article, the convex formulation in (2) is applied for retrieving the sparse and low-rank components from the given $\mathbf{C}$.

B. Affine Varieties and Tangent Spaces

In the seminal work [37], the convex optimization problem (2) without the constraints $\mathbf{S}^T = -\mathbf{S}$ and $\mathbf{L}^T = -\mathbf{L}$ is considered, which provided sufficient conditions to retrieve $\tilde{\mathbf{S}}$ and $\tilde{\mathbf{L}}$ exactly. The results in [37] established results for general square matrices with a real field. In this section, we extend the results to skew symmetric matrices in real field, $\mathbb{S}^n$. In order to address the decomposition, we consider the sparse matrix sets as an affine variety and low-rank matrix sets as a manifold. We characterize the necessary and sufficient conditions required for the unique decomposition in terms of the tangent space to the affine variety of support constrained skew symmetric matrices at $\tilde{\mathbf{S}}$–the original sparse matrix–and the tangent space to the manifold of rank constrained skew symmetric matrices at $\tilde{\mathbf{L}}$–the original low-rank matrix. Note that an affine variety is defined as the zero set of a system of polynomial equations [41].

Remark 2: The skew symmetric matrices with real entries have the property that all the non-zero eigenvalues are pure imaginary and they exist in conjugate pairs. Therefore, the rank r of every skew symmetric matrix must be *even*, and the multiplicity of the singular values must be a positive multiple of two.

Next, we provide definitions of tangent spaces, specific to skew symmetric matrices in real field, as our major focus in this article is on imaginary part of Hermitian matrices. The affine variety of skew symmetric matrices constrained by support size m is defined as:

$$\mathcal{S}(m) := \{\mathbf{M} \in \mathbb{S}^n : |support(\mathbf{M})| \leqslant m\}. \tag{3}$$

Notice that $\mathcal{S}(m)$ is defined over the space of all skew symmetric matrices, $\mathbb{S}^n$, i.e., the set of all matrices $\mathbf{M} \in \mathbb{R}^{n\times n}$ with $\mathbf{M}^T = -\mathbf{M}$. We establish the following result on tangent spaces of sparse real skew symmetric matrices.

Lemma 1: For any skew symmetric matrix $\mathbf{M} \in \mathbb{S}^n$, the tangent space $\Omega(\mathbf{M})$ with respect to $\mathcal{S}(|support(\mathbf{M})|)$ at $\mathbf{M}$ is:

$$\Omega(\mathbf{M}) := \{\mathbf{N} \in \mathbb{S}^n : support(\mathbf{N}) \subseteq support(\mathbf{M})\}. \tag{4}$$

Proof: See Appendix A. ∎

The dimension of this tangent space is $support(\mathbf{M})/2$ owing to the skew symmetric property.

We define set of skew symmetric matrices of rank r as:

$$\mathcal{R}(r) := \{\mathbf{M} \in \mathbb{S}^n : rank(\mathbf{M}) = r\}. \tag{5}$$

It is shown in [42] that $\mathcal{R}(r)$ is a differential manifold, whose dimension is $nr - \frac{r^2-r}{2}$.

Lemma 2: For any skew symmetric matrix $\mathbf{M} \in \mathbb{S}^n$, the tangent space $T(\mathbf{M})$ with respect to $\mathcal{R}(rank(\mathbf{M}))$ at $\mathbf{M}$ is:

$$T(\mathbf{M}) := \{\mathbf{U}\mathbf{X}^T - \mathbf{X}\mathbf{U}^T : \mathbf{X} \in \mathbb{R}^{n\times r}\}, \tag{6}$$

where $\mathbf{M} = \mathbf{U}\mathbf{D}\mathbf{V}^T$ is the compact singular value decomposition (CSVD) of $\mathbf{M}$.

Proof: See Appendix B. ∎

The dimension of $T(\mathbf{M})$ is $nr - \frac{r^2}{2}$.

The following lemma is obtained based on Remark 2.

Lemma 3: Let $\mathbf{M} \in \mathbb{S}^n$ be a skew symmetric matrix and let $\mathbf{M} = \mathbf{U}\mathbf{D}\mathbf{V}^T$ be CSVD of $\mathbf{M}$, $\mathbf{D} := diag(\sigma_1, \ldots, \sigma_r)$ with $\sigma_1 \geqslant \sigma_2 \geqslant \cdots \geqslant \sigma_r$, where r is the rank of $\mathbf{M}$. Then, the projection matrices $\mathbf{U}\mathbf{U}^T$ and $\mathbf{V}\mathbf{V}^T$ of the given skew symmetric matrix $\mathbf{M}$ are equal.

Proof: See supplementary material, Appendix A or [43]. ∎

Suppose we have prior information about $\Omega(\tilde{\mathbf{S}})$ and $T(\tilde{\mathbf{L}})$, in addition to being given $\mathbf{C} = \tilde{\mathbf{S}} + \tilde{\mathbf{L}}$. Then, it can be shown that a necessary and sufficient condition for unique identifiability of $(\tilde{\mathbf{S}}, \tilde{\mathbf{L}})$ in terms of the tangent spaces is

$$\Omega(\tilde{\mathbf{S}}) \cap T(\tilde{\mathbf{L}}) = \{\mathbf{0}\}, \tag{7}$$

i.e., the tangent spaces $\Omega(\tilde{\mathbf{S}})$ and $T(\tilde{\mathbf{L}})$ has trivial intersection. In other words, if the tangent spaces intersect only at origin, then we can retrieve the component matrices $\tilde{\mathbf{S}}$ and $\tilde{\mathbf{L}}$, if we have access to $\Omega(\tilde{\mathbf{S}})$ and $T(\tilde{\mathbf{L}})$. Given exact characterization of tangent spaces for real skew symmetric matrices in Lemma 1 and Lemma 2, it is possible to test for the necessary and sufficient trivial intersection condition for a given matrix $\mathbf{M}$. Now, analogous to development in [37], we obtain the sparse and low-rank decomposition using convex optimization.

0018-9286 (c) 2021 IEEE. Personal use is permitted, but republication/redistribution requires IEEE permission. See http://www.ieee.org/publications_standards/publications/rights/index.html for more information.
Authorized licensed use limited to: University of Minnesota. Downloaded on August 12,2022 at 21:08:33 UTC from IEEE Xplore. Restrictions apply.

This article has been accepted for publication in a future issue of this journal, but has not been fully edited. Content may change prior to final publication. Citation information: DOI 10.1109/TAC.2021.3124979, IEEE Transactions on Automatic Control

C. Sparse plus low-rank Decomposition using Optimization

In general, it is not possible to recover the original sparse and low-rank matrices by solving (2). To begin with, the solution of the optimization problem depends intricately on the penalty factor $\boldsymbol{\gamma}$. In Proposition 3, we prove that for $\boldsymbol{\gamma}$ close to zero the optimal solution $(\widehat{\mathbf{S}}_{\boldsymbol{\gamma}}, \widehat{\mathbf{L}}_{\boldsymbol{\gamma}})$ returned by (2) is $(\mathbf{C}, \mathbf{0})$, whereas for $\boldsymbol{\gamma}$ sufficiently large $(\widehat{\mathbf{S}}_{\boldsymbol{\gamma}}, \widehat{\mathbf{L}}_{\boldsymbol{\gamma}}) = (\mathbf{0}, \mathbf{C})$.

Another issue in decomposing the given matrix $\mathbf{C}$ is if either $\tilde{\mathbf{S}}$ is low-rank, or $\tilde{\mathbf{L}}$ is sparse. For example, suppose that the low-rank matrix $\tilde{\mathbf{L}}$ is such that $\tilde{\mathbf{L}}_{11} \neq 0$ with every other entry zero, and $\tilde{\mathbf{S}}$ be any sparse matrix with $\tilde{\mathbf{S}}_{11} \neq 0$. Then, the optimization may return $(\mathbf{C}, \mathbf{0})$ or $(\mathbf{0}, \mathbf{C})$ as the solution depends on the rank of $\tilde{\mathbf{S}}$. Another example where the unique decomposition is not possible is when $\tilde{\mathbf{S}}$ has support restricted to the first column and the first column of $\tilde{\mathbf{L}}$ negates all the entries of $\mathbf{S}$. Then, a reasonable solution is $(\mathbf{0}, \mathbf{C})$.

Next, we characterize the optimal regions of (2) and provide sufficient conditions under which it obtain the unique decomposition, i.e., returns the true sparse and low-rank matrices. The following proposition provides a sufficient condition for (2) to return the optimum solution $(\widehat{\mathbf{S}}_{\boldsymbol{\gamma}}, \widehat{\mathbf{L}}_{\boldsymbol{\gamma}}) = (\tilde{\mathbf{S}}, \tilde{\mathbf{L}})$.

Proposition 1: Suppose that $\mathbf{C} = \tilde{\mathbf{S}} + \tilde{\mathbf{L}}$, $\mathbf{C} \neq \mathbf{0}$ where $\tilde{\mathbf{S}}, \tilde{\mathbf{L}} \in \mathbb{S}^n$ is given. Then, $(\tilde{\mathbf{S}}, \tilde{\mathbf{L}})$ is the unique optimizer of (2) if the following conditions are satisfied:

1) $\Omega(\tilde{\mathbf{S}}) \cap T(\tilde{\mathbf{L}}) = \{\mathbf{0}\}$.
2) There exist duals $\mathbf{Q}_1, \mathbf{Q}_2 \in \mathbb{R}^{n \times n}$ such that
   (a) $P_{\Omega(\tilde{\mathbf{S}})}(\mathbf{Q}_1 - \mathbf{Q}_2 - \mathbf{Q}_2^T) = \gamma sign(\tilde{\mathbf{S}})$,
   (b) $P_{T(\tilde{\mathbf{L}})}(\mathbf{Q}_1) = \mathbf{U}\mathbf{V}^T$,
   (c) $\|P_{\Omega(\tilde{\mathbf{S}})^C}(\mathbf{Q}_1 - \mathbf{Q}_2 - \mathbf{Q}_2^T)\|_\infty < \gamma$,
   (d) $\|P_{T^\perp}(\mathbf{Q}_1)\|_2 < 1$,

where $P_{\Omega(\tilde{\mathbf{S}})}(\mathbf{M})$ is obtained by setting entries of $\mathbf{M}$ outside the support of $\tilde{\mathbf{S}}$ to zero and projecting it to the space of skew symmetric matrices, and $P_{T(\tilde{\mathbf{L}})}(\mathbf{M}) := P_{\mathbf{U}}\mathbf{M} + \mathbf{M}P_{\mathbf{U}} - P_{\mathbf{U}}\mathbf{M}P_{\mathbf{U}}$; $P_{\mathbf{U}} = \mathbf{U}\mathbf{U}^T$, $\tilde{\mathbf{L}} = \mathbf{U}\Sigma\mathbf{V}^T$.

Proof: See supplementary material, Appendix B or [43]. ■

D. Sufficient Conditions to Retrieve $\tilde{\mathbf{S}}$ and $\tilde{\mathbf{L}}$

Here, we provide some sufficient conditions that guarantee the existence of the duals $\mathbf{Q}_1$ and $\mathbf{Q}_2$ discussed in Proposition 1. The definitions $\mu(\tilde{\mathbf{S}}) := \max_{\mathbf{N} \in \Omega(\tilde{\mathbf{S}}): \|\mathbf{N}\|_\infty \leqslant 1} \|\mathbf{N}\|_2$ and $\xi(\tilde{\mathbf{L}}) := \max_{\mathbf{N} \in T(\tilde{\mathbf{L}}): \|\mathbf{N}\|_2 \leqslant 1} \|\mathbf{N}\|_\infty$ are used to characterize the properties of the tangent spaces.

Remark 3: Our definitions of $\mu(\tilde{\mathbf{S}})$ and $\xi(\tilde{\mathbf{L}})$ are different from the respective definitions in [37]. In fact, the values of our μ and ξ are less than or equal to the respective values in [37].

The following proposition provides a sufficient condition to obtain the unique decomposition.

Proposition 2: Suppose that $\mathbf{C} = \tilde{\mathbf{S}} + \tilde{\mathbf{L}}$ is given. Suppose that $\mu(\tilde{\mathbf{S}})\xi(\tilde{\mathbf{L}}) < \frac{1}{6}$. Then, the unique optimum for (2) is $(\widehat{\mathbf{S}}_{\boldsymbol{\gamma}}, \widehat{\mathbf{L}}_{\boldsymbol{\gamma}}) = (\tilde{\mathbf{S}}, \tilde{\mathbf{L}})$ if

$$\boldsymbol{\gamma} \in \left(\frac{\xi(\tilde{\mathbf{L}})}{1 - 4\mu(\tilde{\mathbf{S}})\xi(\tilde{\mathbf{L}})}, \frac{1 - 3\mu(\tilde{\mathbf{S}})\xi(\tilde{\mathbf{L}})}{\mu(\tilde{\mathbf{S}})} \right). \tag{8}$$

Proof: See supplementary material, Appendix C or [43]. ■

Remark 4: The range of values in (8) is a superset of the range specified in [37]. In the worst case, (8) would return the same interval specified in [37], due to difference in definitions of the tangent spaces, $\Omega(\tilde{\mathbf{S}})$ and $T(\tilde{\mathbf{L}})$.

Next, we define deg_{max} of a matrix $\mathbf{M}$ as $deg_{max}(\mathbf{M}) := \max\left(\max_{1 \leqslant i \leqslant n}\left(\sum_{j=1}^n \mathbb{1}_{\{\mathbf{M}_{ij} \neq 0\}}\right), \max_{1 \leqslant j \leqslant n}\left(\sum_{i=1}^n \mathbb{1}_{\{\mathbf{M}_{ij} \neq 0\}}\right)\right)$, where $\mathbb{1}_{\{x \neq 0\}} := 1$ if $x \neq 0$ and $\mathbb{1}_{\{x \neq 0\}} := 0$ if $x = 0$ denotes the indicator function. We define the *maximum incoherence* of the row/column space of the real skew symmetric matrix $\mathbf{M}$ as $inc(\mathbf{M}) := \max_k \|\mathbf{U}\mathbf{U}^T e_k\|_2$, where $\mathbf{U}\Sigma\mathbf{V}^T$ is the CSVD of $\mathbf{M}$. This definition is different from the one in [37] due to Lemma 3.

The following lemma extends the sufficient condition in Proposition 2 in terms of deg_{max} and maximum incoherence.

Lemma 4: Let $\mathbf{C} = \tilde{\mathbf{S}} + \tilde{\mathbf{L}}$ with $deg_{max}(\tilde{\mathbf{S}})$ and $inc(\tilde{\mathbf{L}})$ as defined above. If $deg_{max}(\tilde{\mathbf{S}})inc(\tilde{\mathbf{L}}) < \frac{1}{12}$, then the unique optimum of the convex program (2) is $(\widehat{\mathbf{S}}_{\boldsymbol{\gamma}}, \widehat{\mathbf{L}}_{\boldsymbol{\gamma}}) = (\tilde{\mathbf{S}}, \tilde{\mathbf{L}})$ for a range of values of γ given by:

$$\gamma \in \left(\frac{2inc(\tilde{\mathbf{L}})}{1 - 8deg_{max}(\tilde{\mathbf{S}})inc(\tilde{\mathbf{L}})}, \frac{1 - 6deg_{max}(\tilde{\mathbf{S}})inc(\tilde{\mathbf{L}})}{deg_{max}(\tilde{\mathbf{S}})} \right). \tag{9}$$

Proof: The proof is similar to Corollary 3 in [37], and is skipped due to space constraint. ■

Thus, by picking a proper γ the convex optimization (2) returns the unique decomposition $(\tilde{\mathbf{S}}, \tilde{\mathbf{L}})$ without the need to determine $\Omega(\tilde{\mathbf{S}})$ and $T(\tilde{\mathbf{L}})$.

Remark 5: Lemma 4 provides a conservative sufficient condition and hence covers only a subclass of uniquely decomposable matrices. In Section VII we provide an example that does not satisfy the sufficient conditions, but still is uniquely decomposable using Algorithm 1, i.e., the network satisfies the transverse intersection (7), but not the sufficient condition in Lemma 4.

It can be observed from the structure of singular vectors in the projection matrix $\mathbf{U}\mathbf{U}^T$ that n must be large for $inc(\tilde{\mathbf{L}})$ to be small enough to satisfy the condition in Lemma 4. Moreover, using the results from [44], it can be shown that the number of non-zero entries in $\tilde{\mathbf{S}}$ must be at most $O(n)$ for the sufficient conditions to hold.

The convex program (2) is equivalent to the following formulation with the mapping $t = \frac{\gamma}{1+\gamma}$, where $t \in [0, 1]$:

$$\begin{aligned} (\widehat{\mathbf{S}}_t, \widehat{\mathbf{L}}_t) \quad = \quad & \arg\min_{\mathbf{S},\mathbf{L}} t\|\mathbf{S}\|_1 + (1-t)\|\mathbf{L}\|_* \\ & \text{subject to } \mathbf{S} + \mathbf{L} = \mathbf{C}, \\ & \qquad \mathbf{S}^T = -\mathbf{S},\ \mathbf{L}^T = -\mathbf{L}. \end{aligned} \tag{10}$$

The following definitions are used to measure the closeness of the estimated matrices with the true matrices.

$$tol_t \quad := \quad \frac{\|\widehat{\mathbf{S}}_t - \tilde{\mathbf{S}}\|_F}{\|\tilde{\mathbf{S}}\|_F} + \frac{\|\widehat{\mathbf{L}}_t - \tilde{\mathbf{L}}\|_F}{\|\tilde{\mathbf{L}}\|_F}, \tag{11}$$

$$diff_t \quad := \quad (\|\widehat{\mathbf{S}}_{t-\epsilon} - \widehat{\mathbf{S}}_t\|_F) + (\|\ \widehat{\mathbf{L}}_{t-\epsilon} - \widehat{\mathbf{L}}_t\|_F), \tag{12}$$

where $\|.\|_F$ denotes the Frobenius norm and $\epsilon > 0$ is a sufficiently small fixed constant. Note that tol_t requires the knowledge of the true matrices $\tilde{\mathbf{S}}$ and $\tilde{\mathbf{L}}$, whereas $diff_t$ does not require any such prior information. Moreover, the mapping between t and $\boldsymbol{\gamma}$ is one-to-one.

In practice, we may not have access to any extra information other than $\mathbf{C}$; thus determining t required for the unique decomposition from Lemma 4 and tol_t becomes difficult. Here we provide guidance on which t (and this γ) to be

0018-9286 (c) 2021 IEEE. Personal use is permitted, but republication/redistribution requires IEEE permission. See http://www.ieee.org/publications_standards/publications/rights/index.html for more information.
Authorized licensed use limited to: University of Minnesota. Downloaded on August 12,2022 at 21:08:33 UTC from IEEE Xplore. Restrictions apply.

This article has been accepted for publication in a future issue of this journal, but has not been fully edited. Content may change prior to final publication. Citation information: DOI 10.1109/TAC.2021.3124979, IEEE Transactions on Automatic Control

employed. The following proposition provides a systematic approach to identify a proper penalty factor t for the unique decomposition.

Proposition 3: Suppose we are given a matrix $\mathbf{C}$, which is obtained by summing $\tilde{\mathbf{S}}$ and $\tilde{\mathbf{L}}$, where $\tilde{\mathbf{S}}$ is a sparse matrix and $\tilde{\mathbf{L}}$ is a low-rank matrix. If $\tilde{\mathbf{S}}$ and $\tilde{\mathbf{L}}$ satisfies $\deg_{\max}(\tilde{\mathbf{S}})inc(\tilde{\mathbf{L}}) < 1/12$, then there exist at least three regions where $diff_t = 0$. In particular, there exists an interval $[t_1, t_2] \subset [0, 1]$ with $0 < t_1 < t_2 < 1$ such that $(\widehat{\mathbf{S}}_t, \widehat{\mathbf{L}}_t) = (\tilde{\mathbf{S}}, \tilde{\mathbf{L}})$ for any $t \in [t_1, t_2]$

Proof: See Appendix C. ∎

Corollary 1: By solving (10) and calculating $diff_t$ for every $t \in \{\varepsilon, 2\varepsilon, \ldots, 1\}$ we obtain $\widehat{\mathbf{S}}_t$ and $\widehat{\mathbf{L}}_t$ and the zero regions specified in Proposition 3, specifically $[t_1, t_2],\ 0 < t_1 < t_2 < 1$, where $diff_t = 0$. For a given $t \in [t_1, t_2]$, if $\deg_{\max}(\hat{\mathbf{S}}_t)inc(\hat{\mathbf{L}}_t) < 1/12$, then the decomposition is exact, that is, $tol_t = 0$ and $(\widehat{\mathbf{S}}_t, \widehat{\mathbf{L}}_t) = (\tilde{\mathbf{S}}, \tilde{\mathbf{L}})$.

Remark 6: Proposition 3 and Corollary 1 are applicable in any general sparse plus low-rank matrix decomposition, and is not restricted to skew symmetric matrix decomposition.

Remark 7: Conversely, if there are only two zero regions, t close to zero and t close to 1, then we can assert that it may not be possible to obtain unique decomposition with this approach. Simulation results show that $t \in [.26, .4]$ is a good region to look for t.

Based on Proposition 3 and Corollary 1, we propose Algorithm 1 to obtain the unique decomposition, which returns the estimated sparse matrix $\widehat{\mathbf{S}}$ and estimated low-rank matrix $\widehat{\mathbf{L}}$.

Remark 8: The aforementioned results can be extended to the space of complex Hermitian matrices also; however, we do not discuss them here.

In the following section, we discuss some preliminaries of linear dynamical systems that are useful in understanding the rest of the article. In Section IV and Section V, we discuss how the matrix decomposition is extremely useful to reconstruct the moral graph/topology of a given linear dynamical model.

III. Linear Dynamical Systems

Consider a linear dynamical system with n interacting agents, each equipped with time-series measurements $(\widetilde{x}_i(t))_{t\in\mathbb{Z}}$, $i \in \{1, \ldots, n\}$, governed by the following linear dynamical model (LDM):

$$\widetilde{\mathbf{x}}(k) = \sum_{l=-\infty}^{\infty} \widetilde{\mathbf{H}}(l)\widetilde{\mathbf{x}}(k-l) + \widetilde{\mathbf{e}}(k), \tag{13}$$

where $\widetilde{\mathbf{x}}(k) = [\widetilde{x}_1(k), \cdots, \widetilde{x}_n(k)]^T$, $\widetilde{\mathbf{e}}(k) = [\widetilde{e}_1(k), \cdots, \widetilde{e}_n(k)]^T$, and for $i, j \in \{1, 2, \cdots, n\},\ i \neq j$, $\widetilde{e}_i(k)$ is a zero mean wide sense stationary (WSS) process uncorrelated with $\widetilde{e}_j(k)$. Additionally, the processes $\{\widetilde{x}_i(k), \widetilde{e}_i(k)\}_{i=1}^n$ are jointly WSS. Let $\mathbf{H}(z) = \mathcal{Z}[\widetilde{\mathbf{H}}(k)]$. Then, $\widetilde{\mathbf{H}}(l) \in \mathbb{R}^{n\times n}$ denotes the weighted adjacency matrix with diagonal entries $\widetilde{\mathbf{H}}_{ii}(l) = 0,\ 1 \leqslant i \leqslant n,\ l \in \mathbb{Z}$, such that $\mathbf{H}$ is well posed, i.e., every entry of $(\mathbf{I} - \mathbf{H}(z))^{-1}$ is analytic on the unit circle, $|z| = 1,\ z \in \mathbb{C}$. An LDM is said to be topologically detectable if $\Phi_{\mathbf{e}}(z)$ is positive definite for every $|z| = 1$. The above model can be represented using the following Transfer Function Model (TFM),

$$\mathbf{x}(z) = \mathbf{H}(z)\mathbf{x}(z) + \mathbf{e}(z),\ z \in \mathbb{C}, \tag{14}$$

where $\mathbf{x}(z) = \mathcal{Z}[\widetilde{\mathbf{x}}(k)]$ and $\mathbf{e}(z) = \mathcal{Z}[\widetilde{\mathbf{e}}(k)]$. In general, there may exist nodes whose observations are not available and remain hidden. These nodes that are not accessible are called hidden/latent/unobservable nodes. $\mathcal{V}_o$ denotes the set of observable nodes with cardinality n_o and $\mathcal{V}_h$ is the set of latent nodes with cardinality n_h.

A. Graphical Representation

The Linear Dynamic Graph (LDG) associated with the LDM (14) is defined as the directed graph $\mathcal{G}(\mathcal{V}, \mathcal{E})$, where $\mathcal{V} = \{1, 2, \cdots, n\}$ and $\mathcal{E} = \{(i, j) | \mathbf{H}_{ji} \neq 0\}$. Thus, there exists a directed edge (i, j) from node i to node j in the LDG if and only if $\mathbf{H}_{ji} \neq 0$. For a directed graph $\mathcal{G}(\mathcal{V}, \mathcal{E})$, parent set of node j is $\mathcal{P}(j) := \{i | (i, j) \in \mathcal{E}\}$, child set of node j is $\mathcal{C}(j) := \{i | (j, i) \in \mathcal{E}\}$ and spouse set of node j is $\mathcal{S}(j) := \{i | i \in \mathcal{P}(\mathcal{C}(j))\}$. Nodes i and j are strict spouses if $i \in \mathcal{S}(j)$, $i \notin \mathcal{C}(j) \cup \mathcal{P}(j)$. The Markov Blanket of node i, denoted $kin(i) := \mathcal{C}(i) \cup \mathcal{P}(i) \cup \mathcal{S}(i)$. The moral or the kin graph, $kin(\mathcal{G}) := \{(i, j) \mid i \in kin(j),\ i, j \in \mathcal{V}\}$, where (i, j) denotes an unordered pair. The topology of $\mathcal{G}$ is defined as an undirected graph $top(\mathcal{G}) := \{(i, j) \mid i \in \mathcal{P}(j) \cup \mathcal{C}(j),\ i, j \in \mathcal{V}\}$.

Similarly, an LDG obtained by restricting the vertex set to the observed nodes is defined by $\mathcal{G}_o(\mathcal{V}_o, \mathcal{E}_o)$, where $\mathcal{E}_o := \{(i, j) | i, j \in \mathcal{V}_o \text{ and } \mathbf{H}_{ji} \neq 0\}$. The topology among the observable nodes, $\mathcal{T}(\mathcal{V}_o, \mathcal{E}_o) := top(\mathcal{G}_o(\mathcal{V}_o, \mathcal{E}_o))$. We define an undirected edge set $\overline{\mathcal{E}}_o := \{(i, j) \mid (i, j) \in \mathcal{E}_o \text{ or } (j, i) \in \mathcal{E}_o,\ i < j\}$. Similarly, the moral graph among the observable nodes is the undirected graph $kin(\mathcal{G}_o) := \{(i, j) \mid i \in kin(j),\ i, j \in \mathcal{V}_o\}$. We define a path between nodes i and j in an undirected graph as a set of nodes $\{i, x_0, \ldots, x_k, j\}$ where $\{(i, x_0), (x_1, x_2), \ldots, (x_{k-1}, x_k)\} \subseteq \mathcal{E}$. We define a path between nodes i and j in an undirected graph as a set of nodes $\{i, x_0, \ldots, x_k, j\}$ where $\{(i, x_0), (x_1, x_2), \ldots, (x_{k-1}, x_k)\} \subseteq \mathcal{E}$. A directed path in a directed graph is a path between nodes i and j with the constraint that all the edges are directed from i towards j. $d_{hop}(i, j)$ is defined for undirected graphs as the number of links between nodes i and j on the shortest path connecting i and j. It can be shown that $d_{hop}(i, j)$ is a metric for undirected graphs. For a node $i \in \mathcal{V}$, the degree of the node is $deg(i) := |\{j \in \mathcal{V} : (i, j) \in \mathcal{E}\}|$. Note that this definition is for undirected edges.

In the next section, we study properties of the IPSDM of a given LDM that are useful in topology/moral graph reconstruction.

IV. Exact Reconstruction of Moral Graph of Observed Nodes and Markov Blanket of Latent Nodes

A. Moral Graph Reconstruction under Complete Observability

In this part of the section we present some important preliminaries for reconstruction of moral graphs from power

0018-9286 (c) 2021 IEEE. Personal use is permitted, but republication/redistribution requires IEEE permission. See http://www.ieee.org/publications_standards/publications/rights/index.html for more information.
Authorized licensed use limited to: University of Minnesota. Downloaded on August 12,2022 at 21:08:33 UTC from IEEE Xplore. Restrictions apply.

This article has been accepted for publication in a future issue of this journal, but has not been fully edited. Content may change prior to final publication. Citation information: DOI 10.1109/TAC.2021.3124979, IEEE Transactions on Automatic Control

spectral density matrices and methods on how to reconstruct moral graph under full observability of the network.

For the graph $\mathcal{G}(\mathcal{V},\mathcal{E})$, the power spectral density matrix (PSDM), $\Phi_{\mathbf{x}}(z)\in\mathbb{C}^{n\times n}$ is given by

$$\Phi_{\mathbf{x}}(z):=\sum_{k=-\infty}^{\infty}\mathbb{E}\{\tilde{\mathbf{x}}(k)\tilde{\mathbf{x}}^T(0)\}z^{-k},\ z\in\mathbb{C},|z|=1. \tag{15}$$

The PSDM and the IPSDM of the dynamical system governed by (14) can be respectively written as (see [13]) $\Phi_{\mathbf{x}}(z)=(\mathbf{I}-\mathbf{H}(z))^{-1}\Phi_{\mathbf{e}}(z)(\mathbf{I}-\mathbf{H}^*(z))^{-1}$ and

$$\Phi_{\mathbf{x}}^{-1}(z)=(\mathbf{I}-\mathbf{H}^*(z))\Phi_{\mathbf{e}}^{-1}(z)(\mathbf{I}-\mathbf{H}(z)). \tag{16}$$

Note that $\Phi_{\mathbf{e}}^{-1}(z)$ is a diagonal matrix, since $\widetilde{e}_i(k)$ is uncorrelated with $\widetilde{e}_\ell(k)$ for $i\neq\ell$.

The following lemma (Theorem 27 in [13]) provides a sufficient condition to estimate the moral graph of $\mathcal{G}(\mathcal{V},\mathcal{E})$ from the IPSDM.

Lemma 5: Consider a well posed and topologically detectable LDM $(\mathbf{H},\mathbf{e})$ with the associated LDG $\mathcal{G}(\mathcal{V},\mathcal{E})$, described by (14), having full node observability. Let IPSDM of $\mathbf{x}$ be given by (16). Then, $[\Phi_{\mathbf{x}}^{-1}]_{i,j}\neq 0$, $i\neq j$ implies $i\in kin(j)$. Moreover, the converse holds almost always.

Remark 9: In [29] and the related works, $[\Phi_{\mathbf{x}}^{-1}]_{i,j}\neq 0$ is considered to be equivalent to nodes i and j being conditionally dependent given the rest of the observations. That is, retrieving conditional dependence is equivalent to reconstructing moral graph.

Remark 10: The results of [29] can be extended to AR models with WSS noise by considering conditional correlation instead of conditional dependence. In this case, retrieving conditional correlation is equivalent to moral graph reconstruction.

B. Structure of the IPSDM with Latent Nodes

In the previous subsection we studied the properties of IPSDM under the assumption that all the nodes are observable. However, topology identification becomes complicated in the presence of latent nodes, often leading to lack of identifiability (see IV-C). Here, we discuss some of the special properties of the IPSDM in the presence of latent nodes that are exploited in this article.

By separating observable nodes and latent nodes, we represent $\mathbf{x}(z)=\begin{bmatrix}\mathbf{x}_o(z)\\ \mathbf{x}_h(z)\end{bmatrix}$ and $\mathbf{e}(z)=\begin{bmatrix}\mathbf{e}_o(z)\\ \mathbf{e}_h(z)\end{bmatrix}$, where $\mathbf{x}_o(z)=\mathcal{Z}[\tilde{\mathbf{x}}_o(k)]$, $\mathbf{x}_h(z)=\mathcal{Z}[\tilde{\mathbf{x}}_h(k)]$, $\mathbf{e}_o(z)=\mathcal{Z}[\tilde{\mathbf{e}}_o(k)]$, and $\mathbf{e}_h(z)=\mathcal{Z}[\tilde{\mathbf{e}}_h(k)]$. The TFM in (14) can be expressed as follows:

$$\begin{bmatrix}\mathbf{x}_o(z)\\ \mathbf{x}_h(z)\end{bmatrix}=\begin{bmatrix}\mathbf{H}_{oo}(z) & \mathbf{H}_{oh}(z)\\ \mathbf{H}_{ho}(z) & \mathbf{H}_{hh}(z)\end{bmatrix}\begin{bmatrix}\mathbf{x}_o(z)\\ \mathbf{x}_h(z)\end{bmatrix}+\begin{bmatrix}\mathbf{e_o}(z)\\ \mathbf{e_h}(z)\end{bmatrix}. \tag{17}$$

Letting $\Phi_{\mathbf{x}}(z)=\begin{bmatrix}\Phi_{oo}(z) & \Phi_{oh}(z)\\ \Phi_{ho}(z) & \Phi_{hh}(z)\end{bmatrix}$ and $\Phi_{\mathbf{x}}^{-1}(z)=\begin{bmatrix}\mathbf{K}_{oo}(z) & \mathbf{K}_{oh}(z)\\ \mathbf{K}_{ho}(z) & \mathbf{K}_{hh}(z)\end{bmatrix}$ we have that (by ignoring the index z) $\Phi_{oo}^{-1}=\mathbf{K}_{oo}-\mathbf{K}_{oh}\mathbf{K}_{hh}^{-1}\mathbf{K}_{ho}$, which follows by applying block matrix inversion formula and using Schur's complement representation [45]. Furthermore, using (16), the IPSDM corresponding to the observed variables can be written as:

$$\Phi_{oo}^{-1}=\mathbf{S}+\mathbf{L},\ \text{where} \tag{18}$$
$$\mathbf{S}=(\mathbf{I}_o-\mathbf{H}_{oo}^*)\Phi_{e_o}^{-1}(\mathbf{I}_o-\mathbf{H}_{oo}), \tag{19}$$
$$\mathbf{L}=\mathbf{H}_{ho}^*\Phi_{e_h}^{-1}\mathbf{H}_{ho}-\Psi^*\Lambda^{-1}\Psi, \tag{20}$$
$$\Psi=\mathbf{H}_{oh}^*\Phi_{e_o}^{-1}(\mathbf{I}-\mathbf{H}_{oo})+(\mathbf{I}-\mathbf{H}_{hh}^*)\Phi_{e_h}^{-1}\mathbf{H}_{ho},\ \text{and}$$
$$\Lambda=\mathbf{H}_{oh}^*\Phi_{e_o}^{-1}\mathbf{H}_{oh}+(\mathbf{I}-\mathbf{H}_{hh}^*)\Phi_{e_h}^{-1}(\mathbf{I}-\mathbf{H}_{hh}).$$

The following proposition shows that $support(\mathbf{S})$ can retrieve the moral graph among the observable nodes, $kin(\mathcal{G}_o)$.

Proposition 4: Consider a well-posed and topologically detectable LDM, $(\mathbf{H},\mathbf{e})$, described by (14), with the associated graph $\mathcal{G}(\mathcal{V},\mathcal{E})$. Let $\mathbf{S}$ be given by (19). Then, the set $\widehat{\mathcal{E}}_o:=\{(i,j)|\mathbf{S}_{ij}\neq 0, i<j\}$ reconstructs $kin(\mathcal{G}_o)$ almost always.

Proof: Notice that (16) and (19) are exactly the same, except $\mathbf{H}$, $\Phi_{\mathbf{e}}$, and $\mathbf{I}$ in (16) are replaced with $\mathbf{H}_{oo}$, $\Phi_{\mathbf{e}_o}$, and $\mathbf{I}_o$ respectively in (19). Thus, by applying Lemma 5 on $\mathbf{S}$, $\widehat{\mathcal{E}}_o$ retrieves $kin(\mathcal{G}_o)$ almost always. ■

The following theorem shows that $\mathbf{S}$ is sparse if the moral graph, $kin(\mathcal{G}_o)$ is sparse, while $\mathbf{L}$ is a low-rank matrix if $n_h << n_o$. This particular structure aids in decomposing Φ_{oo}^{-1} into $\mathbf{S}$ and $\mathbf{L}$ (or more precisely $\Im\{\Phi_{oo}^{-1}\}$ into $\Im\{\mathbf{S}\}$ and $\Im\{\mathbf{L}\}$ using the results from Section II). Notice that the index z is omitted from the notations. The results hold for every $|z|=1$ uniformly.

Theorem 1: Consider the LDG $\mathcal{G}(\mathcal{V},\mathcal{E})$ described by (14). Let $\mathcal{G}_o(\mathcal{V}_o,\mathcal{E}_o)$ be the LDG, $\mathcal{G}(\mathcal{V},\mathcal{E})$, restricted to the observed nodes. The following holds:

$$|support(\mathbf{S})|\leqslant 2|\mathcal{E}_o|+2|\mathcal{E}_o^{ss}|+n,\ rank(\mathbf{L})\leqslant 2n_h, \tag{21}$$

where $\mathcal{E}_o^{ss}$ denotes the set of undirected edges between the observable strict spouses with a common observable child.

Proof: See Appendix D. ■

Remark 11: Here, we are interested in the scenarios where $2|\mathcal{E}_o|+2|\mathcal{E}_o^{ss}|=O(n)$; note that the maximum number of interconnections in a graph of n nodes is n^2. In this sense, $\mathbf{S}$ is considered *sparse*. If we can uniquely decompose $\Phi_{oo}^{-1}(z)$ into the sparse matrix $\mathbf{S}$ and the low-rank matrix $\mathbf{L}$, then one can obtain $kin(\mathcal{G}_o)$ from $\mathbf{S}$ (see Proposition 4) and the Markov Blanket of the hidden nodes from $\mathbf{L}$ (see Section IV-D). Further, in Section V-B, we reconstruct the exact topology of the entire network, including that of hidden nodes, under some assumptions. However, there are certain identifiability issues related to hidden nodes, inherent in network topology, which make the detection of hidden nodes from $\mathbf{L}$ difficult, even impossible in some cases. We address them next.

C. Identifiability of Latent Nodes

Here, we discuss identifiability of the hidden nodes inherent to the graph structure and not limited to any specific reconstruction method. We illustrate the non-identifiability via examples.

Fig. 1a and Fig. 1d represent LDGs with LDMs given by $\widetilde{x}_1=\widetilde{e}_1$, $\widetilde{x}_2=\widetilde{x}_1+\sum_{i=4}^n h_{2i}*\widetilde{x}_i(k)+\widetilde{e}_2$, $\widetilde{x}_3=h_{32}*\widetilde{x}_2(k)+\widetilde{e}_3$, where node 1 is latent, and $\widetilde{x}_2=\sum_{i=4}^n h_{2i}*\widetilde{x}_i(k)+$

0018-9286 (c) 2021 IEEE. Personal use is permitted, but republication/redistribution requires IEEE permission. See http://www.ieee.org/publications_standards/publications/rights/index.html for more information.
Authorized licensed use limited to: University of Minnesota. Downloaded on August 12,2022 at 21:08:33 UTC from IEEE Xplore. Restrictions apply.

This article has been accepted for publication in a future issue of this journal, but has not been fully edited. Content may change prior to final publication. Citation information: DOI 10.1109/TAC.2021.3124979, IEEE Transactions on Automatic Control

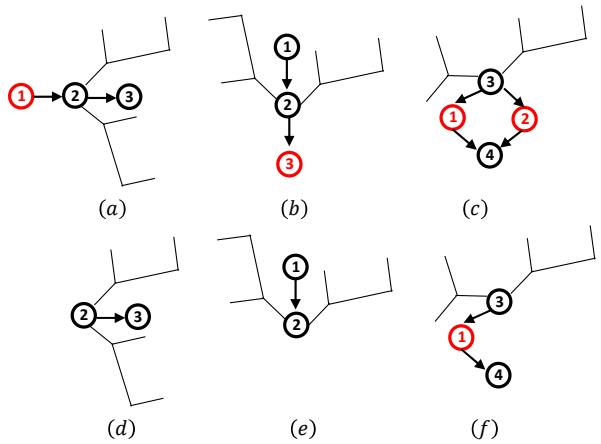

Fig. 1: Non-identifiability of hidden nodes (red colored nodes): (a) hidden node is terminal and strict parent (b) hidden node is terminal and strict child (c) Markov Blankets of hidden nodes 1 and 2 overlapped.

$\hat{e}_2,\ \widetilde{x}_3 = h_{32} * \widetilde{x}_2(k) + \widetilde{e}_3$ respectively. Let $\hat{e}_2 = \widetilde{e}_2 + \widetilde{e}_1$. Then the observed node time-series obtained from the two LDMs are identical and the two models are indistinguishable from Φ_{oo}^{-1}.

Similarly, consider the LDGs shown in Fig. 1b and Fig. 1e with LDMs given by $\widetilde{x}_1 = \widetilde{e}_1,\ \widetilde{x}_2 = \widetilde{x}_1 + \sum_{i=4}^{n} h_{2i} * \widetilde{x}_i(k) + \widetilde{e}_2,\ \widetilde{x}_3 = h_{32} * \widetilde{x}_2(k) + \widetilde{e}_3,\ \widetilde{x}_1 = \widetilde{e}_1,\ \widetilde{x}_2 = \widetilde{x}_1 + \sum_{i=4}^{n} h_{2i} * \widetilde{x}_i(k) + \widetilde{e}_2$ respectively, where node 3 is latent. Again, the time-series among the observable nodes obtained from both the LDGs are the same and hence the two models are indistinguishable.

Based on the aforementioned discussion, we make the following assumptions for identifiability of a hidden node.

Assumption 1: Any hidden node k_h in $\mathcal{G}(\mathcal{V}, \mathcal{E})$ has at least one observed-child $c \in \mathcal{V}_o$. Further, k_h is a parent or child of another observable node $j \in \mathcal{V}_o \backslash \{c\}$.

We next illustrate that non-identifiability issues arise when the Markov Blankets of hidden nodes overlap. Consider the LDGs shown in Fig. 1c and Fig. 1f with LDMs given by $\widetilde{x}_3 = \sum_{i=5}^{n} h_{3i} * \widetilde{x}_i(k) + \widetilde{e}_3,\ \widetilde{x}_1 = \widetilde{x}_3 + \widetilde{e}_1,\ \widetilde{x}_2 = \widetilde{x}_3 + \widetilde{e}_2,\ \widetilde{x}_4 = \widetilde{x}_1 + \widetilde{x}_2 + \widetilde{e}_4$, and $\widetilde{x}_3 = \sum_{i=5}^{n} h_{3i} * \widetilde{x}_i(k) + \widetilde{e}_3,\ \widetilde{x}_1 = \widetilde{x}_3 + \hat{e}_1,\ \widetilde{x}_4 = \widetilde{x}_1 + \widetilde{e}_4$, where $\hat{e}_1 = \widetilde{e}_1 + \widetilde{x}_2$, respectively, where nodes 1 and 2 are latent. Both LDMs result in the same observed time-series, which leads to non-identifiability of hidden node 2. Hence, we make the following assumption about the spatial distribution of hidden nodes in the LDG $\mathcal{G}(\mathcal{V}, \mathcal{E})$.

Assumption 2: For every distinct $k_h, k_h' \in \mathcal{V}_h$, $d_{hop}(k_h, k_h') > 4$.

Assumption 2 is sufficient to ensure that Markov Blankets of any two distinct hidden nodes k_h and k_h' do not overlap. When the intersection of the Markov Blankets of k_h and $k_{h'}$ contain more than one observable node, then one of the hidden nodes k_h or $k_{h'}$ is non-identifiable (see the illustration associated with Fig. 1c). If the intersection has at most one node, then both the hidden nodes might be identifiable. We make a slightly more conservative assumption that the Markov Blankets of the hidden nodes are non-overlapping. Moreover, the implication of Assumption 2 is that the Markov Blanket of a hidden node $h \in \mathcal{V}_h$ is $\{\mathcal{P}(h) \cup \mathcal{C}(h) \cup \mathcal{S}(h)\} \subseteq \mathcal{V}_o$.

Remark 12: Note that Assumption 2 might seem stronger than Assumption 2 in [17]. However, [17] restricted attention to radial topologies associated with bi-directed LDGs and assumed that the hidden nodes are at least three hops away from the leaf nodes. On the contrary, algorithms in Section V can reconstruct more general linear dynamical networks, including loopy networks.

D. Markov Blanket Reconstruction of the Latent nodes

Here, we provide the following definition and theorems which helps in learning the Markov Blanket of hidden nodes.

Definition 1: For $i, j \in \mathcal{V}_o$ and hidden node $h \in \mathcal{V}_h$, define $DE_h(i,j) := \{g_1, g_2, g_3, g_4, g_5, g_6, g_7, g_8, g_9\},\ DE_h^{ss}(i,j) := \{g_{10}, g_{11}\}$, and $DM_h(i,j) := DE_h(i,j) \cup DE_h^{ss}(i,j)$, where $i \to h$ is denoted as (i,h) with $g_1 = \{(h,i),(h,j)\},\ g_2 = \{(h,i),(j,h)\},\ g_3 = \{(h,i),(h,k),(j,k)\},\ \forall k \in \mathcal{V}_o \backslash \{i,j\},\ g_4 = \{(i,h),(h,j)\},\ g_5 = \{(i,h),(h,k),(j,k)\},\ \forall k \in \mathcal{V}_o \backslash \{i,j\},\ g_6 = \{(i,k),(h,k),(j,h)\},\ \forall k \in \mathcal{V}_o \backslash \{i,j\},\ g_7 = \{(i,k),(h,k),(h,j)\},\ \forall k \in \mathcal{V}_o \backslash \{i,j\},\ g_8 = \{(h,i),(j,i)\},\ g_9 = \{(h,j),(i,j)\},\ g_{10} = \{(i,h),(j,h)\}$, and $g_{11} = \{(i,k_1),(h,k_1),(h,k_2),(k_2,j)\},\ \forall k_1, k_2 \in \mathcal{V}_o \backslash \{i,j\}$.

$DM_h(i,j)$ enumerates all the possible paths between two observable nodes i, j present in the Markov Blanket of hidden node h. We now present a result which infers the Markov Blanket of a hidden node h in $\mathcal{G}(\mathcal{V}, \mathcal{E})$ from $support(\mathbf{L})$.

Theorem 2: Suppose the LDM in (17) satisfies assumptions 1, 2. Let $\mathbf{L}$ be given by (20) and let $i, j \in \mathcal{V}_o,\ i \neq j$. Then, the following statements hold:

(a) If $\mathbf{L}_{ij} \neq 0$, then there exists $g \in DM_h(i,j)$ such that $g \in \mathcal{G}(\mathcal{V}, \mathcal{E})$, for some $h \in \mathcal{V}_h$. Further, $d_{hop}(i,h) \leqslant 2$ and $d_{hop}(j,h) \leqslant 2$.

(b) Given $\mathbf{L}_{ij} \neq 0$, suppose there exist $g_1 \in DM_{h_1}(i,j)$ and $g_2 \in DM_{h_2}(i,j)$ connecting i and j such that $g_1, g_2 \in \mathcal{G}(\mathcal{V}, \mathcal{E})$, for some $h_1, h_2 \in \mathcal{V}_h$. Then $h_1 = h_2$.

Proof: See Appendix F. ■

Remark 13: We note that, for a set of system parameters, noise statistics can be construed such that a $g \in DM_h(i,j)$ is present in the LDG $\mathcal{G}(\mathcal{V}, \mathcal{E})$, with $\mathbf{L}_{ij} = 0$. We remark that such cases are pathological; we will assume that the converse of Theorem 2(a) holds almost everywhere.

Thus, based on the locations of non-zero entries in $\mathbf{L}$, we construct $V_H = \{i | i \in \mathcal{V}_o, \exists k \in \mathcal{V}_o \backslash \{i\} \text{ s.t. } \mathbf{L}_{ik} \neq 0\}$ and $E_H = \{(i,j) | i, j \in V_H, \mathbf{L}_{ij} \neq 0\}$. The following result shows that (V_H, E_H) is a disjoint collection of connected undirected subgraphs (see Fig. 4b for example). Moreover, the number of connected undirected subgraphs in E_H is equal to number of hidden nodes n_h in the LDG $\mathcal{G}(\mathcal{V}, \mathcal{E})$.

Theorem 3: Suppose the LDM in (17) satisfies assumptions 1, 2. Let $\mathbf{L}$ be given by (20). From $\mathbf{L}$, construct the following: $V_H = \{i | i \in \mathcal{V}_o, \exists k \in \mathcal{V}_o \backslash \{i\} \text{ s.t. } \mathbf{L}_{ik} \neq 0\}$, $E_H = \{(i,j) | i, j \in V_H, \mathbf{L}_{ij} \neq 0\}$. For every hidden node $l \in \mathcal{V}_h$, let

0018-9286 (c) 2021 IEEE. Personal use is permitted, but republication/redistribution requires IEEE permission. See http://www.ieee.org/publications_standards/publications/rights/index.html for more information.
Authorized licensed use limited to: University of Minnesota. Downloaded on August 12,2022 at 21:08:33 UTC from IEEE Xplore. Restrictions apply.

This article has been accepted for publication in a future issue of this journal, but has not been fully edited. Content may change prior to final publication. Citation information: DOI 10.1109/TAC.2021.3124979, IEEE Transactions on Automatic Control

$M_l = \mathcal{P}(l) \cup \mathcal{C}(l) \cup \mathcal{S}(l), Q_l = \{(i,j) | i,j \in M_l, \mathbf{L}_{ij} \neq 0\}$. Then

(a) $M_{l_1} \bigcap M_{l_2} = \varnothing$, for all $l_1, l_2 \in \mathcal{V}_h, l_1 \neq l_2$.
(b) $Q_{l_1} \bigcap Q_{l_2} = \varnothing$, for all $l_1, l_2 \in \mathcal{V}_h, l_1 \neq l_2$.
(c) $V_H = \bigcup_{l=1}^{n_h} M_l$.
(d) $E_H = \bigcup_{l=1}^{n_h} Q_l$.

Proof: See Appendix G. ∎

Remark 14: The above theorem estimates the number of hidden nodes n_h as the number of connected undirected subgraphs in E_H. Each connected component (M_l, Q_l) is due to a hidden node $l \in \mathcal{V}_h$, that is, M_l is the Markov Blanket of l in $\mathcal{G}(\mathcal{V}, \mathcal{E})$, while Q_l is an undirected edge set that contain edges among any two distinct nodes in M_l.

E. Moral Graph Reconstruction of Observable Nodes and Localization of Hidden Nodes from Φ_{oo}^{-1}

As shown in Theorem 1, $\mathbf{S}$ is sparse and $\mathbf{L}$ is low-rank. Then, one can retrieve $\mathbf{S}$ and $\mathbf{L}$ from Φ_{oo}^{-1} by employing the following optimization.

$$\begin{aligned}(\widehat{\mathbf{S}}_{\boldsymbol{\gamma}}, \widehat{\mathbf{L}}_{\boldsymbol{\gamma}}) \quad = \quad & \arg \min_{\mathbf{S},\mathbf{L} \in \mathbb{C}^{n \times n}} \boldsymbol{\gamma} \|\mathbf{S}\|_1 + \|\mathbf{L}\|_* \\ & \text{subject to } \mathbf{S} + \mathbf{L} = \Phi_{oo}^{-1}, \\ & \qquad \mathbf{S} - \mathbf{S}^* = \mathbf{0},\ \mathbf{L} - \mathbf{L}^* = \mathbf{0}.\end{aligned} \tag{22}$$

Section II has provided certain sufficient conditions for the unique decomposition, in the space of skew symmetric matrices. As mentioned in Remark 8, one can extend the results to the space of complex Hermitian matrices also, which can be applied to solve (22). Then, $support(\widehat{\mathbf{S}}_\gamma)$ recovers the exact moral graph among the observable nodes, $kin(\mathcal{G}_o)$, and $rank(\widehat{\mathbf{L}}_\gamma)$ provides a lower bound on the number of hidden nodes. Additionally, as shown in Theorem 3, $support(\widehat{\mathbf{L}}_\gamma)$ retrieves Markov Blankets of all the hidden nodes.

F. Reconstruction based on $\Im\{\Phi_{oo}^{-1}(z)\}$

In Theorem 1, it was shown that $\mathbf{S}$ is sparse and $\mathbf{L}$ is low-rank, which implies that the same applies respectively to $\Im\{\mathbf{S}\}$ and $\Im\{\mathbf{L}\}$. Based on Theorem 1, one can show that $|support(\Im\{\mathbf{S}\})| \leqslant 2|\mathcal{E}_o| + 2|\mathcal{E}_o^{ss}|$ and $rank(\Im\{\mathbf{L}\}) \leqslant 4n_h$. Therefore, $\Im\{\mathbf{S}\}$ is sparse and $\Im\{\mathbf{L}\}$ is low-rank. As Φ_{oo}^{-1} is Hermitian, $\Im\{\Phi_{oo}^{-1}\}$ is skew symmetric, and hence the results from Section II are applicable here. Then, by applying the convex optimization (10) with $\mathbf{C} = \Im\{\Phi_{oo}^{-1}(z)\}$, one can retrieve the ground truth $\Im\{\mathbf{S}(z)\}$ and $\Im\{\mathbf{L}(z)\}$, for all $|z| = 1$, and appropriately selected $\boldsymbol{\gamma}$ as shown in Section II. This procedure is provided in Algorithm 1. The caveat of decomposing $\Im\{\Phi_{oo}^{-1}\}$ is that the following assumption is required for consistent moral graph/topology reconstruction from $\Im\{\mathbf{S}\}$ and $\Im\{\mathbf{L}\}$.

Assumption 3: For any $1 \leqslant i, k \leqslant n$, $i \neq k$, if $\mathbf{H}_{ik}(z) \neq 0$, then $\Im\{\mathbf{H}_{ik}(z)\} \neq 0$, for all z, $|z| = 1$.

Remark 15: Assumption 3 is necessary to reconstruct $kin(\mathcal{G}_o)$ and the Markov Blankets of the hidden nodes from the decomposition of $\Im\{\Phi_{oo}^{-1}\}$, instead of decomposing Φ_{oo}^{-1} directly. From (19), (20), it follows that $\Im\{\mathbf{S}\}$ and $\Im\{\mathbf{L}\}$ depend on elements of $\Im\{\mathbf{H}\}$. Hence, when Assumption 3 holds, the Lemma 5, Proposition 4, Theorem 1, 2, and 3 hold by replacing Φ_x^{-1}, Φ_{oo}^{-1}, $\mathbf{S}$, and $\mathbf{L}$ with $\Im\{\Phi_x^{-1}\}$, $\Im\{\Phi_{oo}^{-1}\}$, $\Im\{\mathbf{S}\}$, and $\Im\{\mathbf{L}\}$ respectively. In other words, $kin(\mathcal{G}_o)$ and the Markov Blanket of hidden nodes can be obtained by decomposing $\Im\{\Phi_{oo}^{-1}\}$ instead of Φ_{oo}^{-1}. We focus on the decomposition of $\Im\{\Phi_{oo}^{-1}\}$ in this article.

Remark 16: $kin(\mathcal{G}_o)$, obtained from $\Im\{\mathbf{S}\}$ using Proposition 4, would contain $top(\mathcal{G}_o)$ as well as additional edges due to strict spouses in $\mathcal{G}_o$. Likewise, (M_l, Q_l) obtained from $support(\Im\{\mathbf{L}\})$ using Theorem 3 may contain edges apart from $P(l) \cup C(l)$ of a hidden node l. Such spurious edges maybe many; examples include bi-directed LDGs. There is a need to eliminate them so that exact recovery of $top(\mathcal{G})$ is possible.

In the next section, we develop techniques to eliminate the spurious edges and reconstruct the exact topology, for a wide class of networks.

V. Exact Topology Reconstruction

In this section, we develop methods for exact recovery of $top(\mathcal{G})$, under Assumption 4, which is applicable to wide class of applications.

A. Elimination of Strict Spouse Edges

Here, we show that, in certain LDMs, the strict spouse edges satisfy properties that can be exploited toward exact topology reconstruction. Notice that for *some* of the results (viz Theorem 4 and Theorem 5), we restrict our interest to the models that satisfy the following assumption. For the networks that satisfy Assumption 4, Theorem 4 will show that $support(\Im\{\mathbf{S}\})$ would reconstruct the exact topology, $top(\mathcal{G}_o)$ (not $kin(\mathcal{G}_o)$).

Assumption 4: For the LDM in (14), and $i, k, l \in \mathcal{V}$, if $\mathbf{H}_{ki}(z) \neq 0$ and $\mathbf{H}_{kl}(z) \neq 0$, then $\angle\mathbf{H}_{ki}(z) = \angle\mathbf{H}_{kl}(z)$.

Remark 17: Assumption 4 is satisfied by a large class of engineering systems. For instance, Section 2 of [14] provides engineering systems that satisfy Assumption 4. Also, other examples include linearized chemical reaction ODEs [46]. For example, see (10.2.2) in [46].

The following lemma (Theorem 3 in [14]) is useful in proving the subsequent results and helps in exploiting additional structure enjoyed by the IPSDM in the networks satisfying Assumption 4.

Lemma 6: Consider a well-posed and topologically detectable LDM $(\mathbf{H}, \mathbf{e})$ with the associated graph $\mathcal{G}(\mathcal{V}, \mathcal{E})$, described by (14), having full node observability and satisfying Assumption 4. If i and j are strict spouses, then $[\Im\{\Phi_{\mathbf{x}}^{-1}\}]_{ij} = 0$.

Lemma 6 eliminates the spurious edges formed due to strict spouse connections by observing the entries of $\Im\{\Phi_x^{-1}\}$. The proof follows from the expansion of (16). Here, $[\Im\{\Phi_x^{-1}\}]_{ij} = 0$ if $\mathbf{H}_{ij} = 0$, $\mathbf{H}_{ji} = 0$, and $\angle\mathbf{H}_{ki} = \angle\mathbf{H}_{kj}$ for all $k \in \mathcal{C}(i) \cap \mathcal{C}(j)$. This can be employed to separate the true parent-child connection from the strict spouse edges in the moral graph obtained from Lemma 5. Combining Lemma 5 and Lemma 6 with Assumption 3, one can conclude that, the undirected graph constructed from $\Im\{\Phi_x^{-1}\}$ is equal to

0018-9286 (c) 2021 IEEE. Personal use is permitted, but republication/redistribution requires IEEE permission. See http://www.ieee.org/publications_standards/publications/rights/index.html for more information.
Authorized licensed use limited to: University of Minnesota. Downloaded on August 12,2022 at 21:08:33 UTC from IEEE Xplore. Restrictions apply.

This article has been accepted for publication in a future issue of this journal, but has not been fully edited. Content may change prior to final publication. Citation information: DOI 10.1109/TAC.2021.3124979, IEEE Transactions on Automatic Control

$top(\mathcal{G})$, if Assumption 4 holds; else it would be $kin(\mathcal{G})$. We use this fact in the following theorem to reconstruct $top(\mathcal{G}_o)$.

Theorem 4: Consider a well-posed and topologically detectable LDM $(\mathbf{H}, \mathbf{e})$ with the associated graph $\mathcal{G}(\mathcal{V}, \mathcal{E})$, described by (14) and satisfying Assumption 4. Let $\mathbf{S}$ be given by (19) and let $\widehat{\mathcal{E}}_o := \{(i,j) : \Im\{\mathbf{S}_{ij}\} \neq 0,\ i < j\}$. Then, $\widehat{\mathcal{E}}_o \subseteq \overline{\mathcal{E}}_o$. Additionally, if the LDM satisfies Assumption 3, then $\widehat{\mathcal{E}}_o = \overline{\mathcal{E}}_o$ almost always.

Proof: See Appendix E. ∎

In the following, we discuss the exact topology reconstruction from $\Im\{\Phi_{oo}^{-1}\}$ based on Theorems 3 and 4.

Algorithm 1 Matrix decomposition

Input: $\Phi_{oo}^{-1}(z)$: IPSDM among $\mathcal{V}_o$, ε, $z = e^{j\omega}$, $\omega \in (-\pi, \pi]$
Output: Matrices $\Im(\mathbf{S}(z))$ and $\Im(\mathbf{L}(z))$

1: Set $\mathbf{C} = \Im\{\Phi_{oo}^{-1}(z)\}$
2: Initialize $(\widehat{\mathbf{S}}_0, \widehat{\mathbf{L}}_0) = (\mathbf{C}, \mathbf{0})$
3: **for all** $t \in \{\varepsilon, 2\varepsilon, \ldots, 1\}$ **do**
4: Solve the convex optimization (10) and calculate $diff_t$ in (12)
5: **end for**
6: Identify the three regions where $diff_t$ is zero and denote the middle region as $[t_1, t_2]$. Pick a $t_0 \in [t_1, t_2]$ and the corresponding pair $(\widehat{\mathbf{S}}_{t_0}, \widehat{\mathbf{L}}_{t_0})$.
7: **if** $deg_{max}(\widehat{\mathbf{S}}_{t_0}) inc(\widehat{\mathbf{L}}_{t_0}) < \frac{1}{12}$ **then**
8: $(\widehat{\mathbf{S}}(z), \widehat{\mathbf{L}}(z)) = (\widehat{\mathbf{S}}_{t_0}, \widehat{\mathbf{L}}_{t_0})$
9: Return $(\widehat{\mathbf{S}}(z), \widehat{\mathbf{L}}(z))$
10: **end if**

B. Reconstruction of $\mathcal{T}(\mathcal{V}, \mathcal{E})$:

The topology, $\mathcal{T}(\mathcal{V}, \mathcal{E})$, of the LDG $\mathcal{G}(\mathcal{V}, \mathcal{E})$ will be reconstructed in three steps: (a) recover the topology restricted to observed nodes given by $\mathcal{T}(\mathcal{V}_o, \mathcal{E}_o)$, (b) determine the number of hidden nodes n_h in the LDG $\mathcal{G}(\mathcal{V}, \mathcal{E})$ and (c) reconstruct the topology associated with each hidden node. We denote the reconstructed topology as $\mathcal{T}(\mathcal{V}_R, \mathcal{E}_R)$. The reconstruction is said to be exact when $\mathcal{T}(\mathcal{V}, \mathcal{E}) = \mathcal{T}(\mathcal{V}_R, \mathcal{E}_R)$.

The first step in topology reconstruction is to obtain $\widehat{\mathbf{S}} = \Im\{\mathbf{S}(z)\}$ and $\widehat{\mathbf{L}} = \Im\{\mathbf{L}(z)\}$ from Algorithm 1. Then, from $\widehat{\mathbf{S}}$, we reconstruct the topology among observed nodes $\mathcal{T}(\mathcal{V}_o, \mathcal{E}_o)$ as shown in Theorem 4. This is performed in Algorithm 2, which reconstructs $\mathcal{T}(\mathcal{V}_o, \mathcal{E}_R)$, where $\mathcal{V}_o$ is the set of observable nodes and $\mathcal{E}_R$ is the undirected edge set reconstructed from $support(\widehat{\mathbf{S}})$. Apart from pathological cases, $\mathcal{T}(\mathcal{V}_o, \mathcal{E}_R)$ is identical to $\mathcal{T}(\mathcal{V}_o, \mathcal{E}_o)$ under Assumption 4.

Remark 18: Algorithms 1 and 2 are applicable for any LDM with Assumption 3 and need not satisfy Assumption 4. However, in that case, $\mathcal{T}(\mathcal{V}_o, \mathcal{E}_R)$ would return $kin(\mathcal{G}_o)$.

Remark 19: As mentioned in Section IV-E, one can decompose the complex Φ_{oo}^{-1} to obtain $\mathbf{S}$ and $\mathbf{L}$, instead of their respective imaginary parts, thus avoiding the need for Assumption 3. $\mathbf{S}$ and $\mathbf{L}$ can then retrieve moral graphs among the observable nodes and Markov Blanket of hidden nodes.

Algorithm 2 Topology reconstruction of observable nodes

Input: $\widehat{\mathbf{S}}(z)$ from Algorithm 1, threshold τ
Output: Reconstructed topology among observable nodes $\mathcal{T}(\mathcal{V}_o, \mathcal{E}_R)$

1: Edge sets $\mathcal{E}_R \leftarrow \{\}$
2: **for all** $(i,j) \in \{1,2,...,n\} \times \{1,2,...,n\}$ **do**
3: **if** $|\widehat{\mathbf{S}}_{ij}(z)| > \tau$ **then**
4: $\mathcal{E}_R \leftarrow \mathcal{E}_R \cup \{(i,j)\}$
5: **end if**
6: **end for**
7: $\mathcal{V}_o \leftarrow \{1, 2, \cdots, n\}$
8: Return $\mathcal{T}(\mathcal{V}_o, \mathcal{E}_R)$

We now proceed with estimating number of hidden nodes and reconstructing the topology associated with hidden nodes using $\Im\{\mathbf{L}\}$.

We emphasize that the undirected edges in Q_l are not necessarily present in the true topology $\mathcal{T}(\mathcal{V}, \mathcal{E})$. The only task remaining in constructing the topology $\mathcal{T}(\mathcal{V}, \mathcal{E})$ is finding the true parents or children of the hidden nodes. For this purpose, we consider each connected component (M_l, Q_l), and reconstruct the topology associated with the hidden node l.

The following result is useful in reconstructing the exact topology associated with hidden node l from *degree* of nodes in (M_l, Q_l). It shows that the information about the degree of each node is *sufficient* to reconstruct the topology associated with the hidden node l.

Theorem 5: Suppose the LDM in (17) satisfies Assumptions 1-4. Consider a hidden node $l \in \mathcal{V}_h$ and its associated undirected graph (M_l, Q_l) as defined in Theorem 3 for $\Im\{\mathbf{L}\}$. Define $\alpha_l := max_{j \in M_l} deg_{M_l}(j)$, where $deg_{M_l}(i) := |\{j \in M_l \backslash i : (i,j) \in Q_l\}|$. The following holds: $\exists k \in M_l$ such that $deg_{M_l}(k) < \alpha_l$ if and only if $|\mathcal{P}(l) \backslash (\mathcal{C}(l) \cup \mathcal{S}(l))| \geqslant 2$ or $|\mathcal{S}(l) \backslash (\mathcal{C}(l) \cup \mathcal{P}(l))| \geqslant 2$ in $\mathcal{G}(\mathcal{V}, \mathcal{E})$.

Proof: See supplementary material, Appendix H or [43]. ∎

Remark 20: From the proof of the above theorem, the following holds:

(a) Consider a node $a_1 \in \mathcal{C}(l) \cup (\mathcal{P}(l) \cap \mathcal{S}(l))$. Then, for every $a_2 \in (\mathcal{C}(l) \cup \mathcal{P}(l) \cup \mathcal{S}(l)) \backslash \{a_1\}$, $(a_1, a_2) \in Q_l$.
(b) Consider a strict spouse, $s_1 \in \mathcal{S}(l) \backslash (\mathcal{C}(l) \cup \mathcal{P}(l))$. Then, for any $a_1 \in \mathcal{C}(l) \cup \mathcal{P}(l)$, $(s_1, a_1) \in Q_l$.
(c) Consider a strict parent, $p_1 \in \mathcal{P}(l) \backslash (\mathcal{C}(l) \cup \mathcal{S}(l))$. Then, for any $a_1 \in \mathcal{C}(l) \cup \mathcal{S}(l)$, $(p_1, a_1) \in Q_l$.

Regardless of the number of strict spouses and strict parents in the LDG, $\mathcal{G}(\mathcal{V}, \mathcal{E})$, for $M_l = \mathcal{C}(l) \cup \mathcal{P}(l) \cup \mathcal{S}(l)$, the following holds from $(a), (b)$ and (c): for $i \in \mathcal{C}(l) \cup (\mathcal{P}(l) \cap \mathcal{S}(l))$ and for $k \in M_l \backslash i$, $(i,k) \in Q_l$. That is, a node from $\mathcal{C}(l) \cup (\mathcal{P}(l) \cap \mathcal{S}(l))$ is connected to every other node from M_l in Q_l. Hence, $deg_{M_l}(i) = |M_l| - 1$ and it is the node with maximum degree. Therefore, $\mathcal{C}(l) \cup \{\mathcal{P}(l) \cap \mathcal{S}(l)\} = \{i | i \in M_l, deg_{M_l}(i) = |M_l| - 1\}$. The nodes in M_l with $deg_{M_l}(i) < |M_l| - 1$ are either strict parents or strict spouses of hidden node l.

0018-9286 (c) 2021 IEEE. Personal use is permitted, but republication/redistribution requires IEEE permission. See http://www.ieee.org/publications_standards/publications/rights/index.html for more information.
Authorized licensed use limited to: University of Minnesota. Downloaded on August 12,2022 at 21:08:33 UTC from IEEE Xplore. Restrictions apply.

This article has been accepted for publication in a future issue of this journal, but has not been fully edited. Content may change prior to final publication. Citation information: DOI 10.1109/TAC.2021.3124979, IEEE Transactions on Automatic Control

We provide the following assumption which is needed for exact reconstruction of topology associated with hidden nodes. When the below assumption is violated, that is, if the number of strict spouse for a hidden node h is one, then there will be a single false edge present in the reconstructed topology associated with the hidden node. Rephrasing, the strict spouse of a hidden node h will be considered as a neighbor in the reconstructed topology associated with the hidden node h. The number of such false edges reconstructed for a network is limited to a maximum of one per hidden node. Nevertheless, to avoid these false edges associated with a hidden node, we make the following assumption.

Assumption 5: In the LDG, $\mathcal{G}(\mathcal{V},\mathcal{E})$, for any hidden node, $h \in \mathcal{V}_h$, if there exists a strict spouse, then there must exist at least one more strict spouse associated with h.

Based on the above theorem and assumption, we propose Algorithm 3, which outputs the reconstructed topology $\mathcal{T}(\mathcal{V}_R,\mathcal{E}_R)$ that is identical to the true topology $\mathcal{T}(\mathcal{V},\mathcal{E})$ of the LDG $\mathcal{G}(\mathcal{V},\mathcal{E})$. The Algorithm 3 consists of three parts as outlined below.

(a) From support of $\Im\{\mathbf{L}\}$, determine V_H and E_H. The graph (V_H,E_H) will be a disjoint collection of connected subgraphs $\bigcup_{l=1}^{n_h}(M_l,Q_l)$. The number of hidden nodes, n_h, is given by the number of connected subgraphs. This is done in steps $1-10$. $\mathcal{V}_H$ and $\mathcal{E}_H$ are both initialized with $\{\}$ (steps $11-12$).

(b) For each (M_l,Q_l), we create a hidden node h_l and add this to $\mathcal{V}_H$ (steps $15-16$). Next, we construct the topology associated with h_l. For this, we compute the degree of each node in (M_l,Q_l) and calculate its maximum, α_l (step 17). We check if there is a node in M_l with degree smaller than α_l. If there is no node in M_l with degree smaller than α_l, then add undirected edge (h_l,i) to $\mathcal{E}_H$ for all $i \in M_l$ (steps $18-28$). Otherwise, we collect the nodes in M_l with degree α_l in the set d_{h_l} and the nodes with degree smaller than α_l in the set $\widetilde{M}_l$ (steps $29-38$). The vertex set $d_{h_l}=\mathcal{C}(h_l)\cup\mathcal{P}(h_l)\cup\mathcal{S}(h_l)$. Thus, add (h_l,i) to $\mathcal{E}_H$ for all $i \in d_{h_l}$ (steps $39-41$). The nodes in $\widetilde{M}_l$ are either strict parents of h_l or strict spouses of h_l in $\mathcal{G}(\mathcal{V},\mathcal{E})$. We find the strict parents from $\widetilde{M}_l$ and add their edges with h_l to $\mathcal{E}_H$ (steps $42-47$).

(c) Repeat (b) for all $l=\{1,2,\cdots,n_h\}$ (step 13). Assign $\mathcal{V}_R$ as $\mathcal{V}_H\cup\mathcal{V}_o$ and $\mathcal{E}_R$ as $\mathcal{E}_H\cup\mathcal{E}_o$ (steps $49-50$). The reconstructed topology of the LDG $\mathcal{G}(\mathcal{V},\mathcal{E})$ is $\mathcal{T}(\mathcal{V}_R,\mathcal{E}_R)$ (step 51).

The reconstructed topology $\mathcal{T}(\mathcal{V}_R,\mathcal{E}_R)$ is identical to the true topology $\mathcal{T}(\mathcal{V},\mathcal{E})$ of the LDG $\mathcal{G}(\mathcal{V},\mathcal{E})$.

Till now, we have investigated topology identification under the assumption that the perfect PSDM is available. However, in practice, we have access only to finite number of observations of the time-series. In the next section, we show that if the number of observations, N, is large enough, then each entry of the estimated IPSDM can be brought ϵ-close to the actual IPSDM. Note that we do not assume the presence of any latent node here. The analysis in this section

Algorithm 3 Full Topology reconstruction with hidden nodes

Input: $\widehat{\mathbf{L}}(z)$ from Algorithm 1, threshold τ and $\mathcal{T}(\mathcal{V}_o,\mathcal{E}_R)$ from Algorithm 2

Output: $\mathcal{T}(\mathcal{V}_R,\mathcal{E}_R)$, reconstructed topology of the LDG $\mathcal{G}(\mathcal{V},\mathcal{E})$

1: $V_H \leftarrow \{\}$
2: $E_H \leftarrow \{\}$
3: **for all** $(i,j) \in \{1,2,...,n\} \times \{1,2,...,n\}$ **do**
4: **if** $|\widehat{\mathbf{L}}_{ij}(z)| > \tau$ **then**
5: $E_H \leftarrow E_H \cup \{(i,j)\}$
6: $V_H \leftarrow V_H \cup \{i,j\}$
7: **end if**
8: **end for**
9: $(V_H,E_H) = \bigcup_{l=1}^{n_h}(M_l,Q_l)$ such that $M_{l_1}\cap M_{l_2} = Q_{l_1}\cap Q_{l_2} = \varnothing$ for all $l_1,l_2 \in \{1,2,...,n_h\}, l_1 \neq l_2$.
10: n_h : number of disjoint connected subgraphs in E_H
11: Vertex set $\mathcal{V}_H \leftarrow \{\}$
12: Edge set $\mathcal{E}_H \leftarrow \{\}$
13: **for all** $l \in \{1,2,...,n_h\}$ **do**
14: flag = 0
15: add a hidden node h_l
16: $\mathcal{V}_H \leftarrow \mathcal{V}_H \cup \{h_l\}$
17: $\alpha_l := max_{j\in M_l} deg_{M_l}(j)$
18: **for all** $i \in M_l$ **do**
19: **if** $deg_{M_l}(i) < \alpha_l$ **then**
20: flag = 1
21: **break**
22: **end if**
23: **end for**
24: **if** flag == 0 **then**
25: **for all** $i \in M_l$ **do**
26: $\mathcal{E}_H \leftarrow \mathcal{E}_H \cup \{(i,h_l)\}$
27: **end for**
28: **end if**
29: **if** flag == 1 **then**
30: $d_{h_l} \leftarrow \{\}$, $\widetilde{M}_l \leftarrow \{\}$
31: **for all** $i \in M_l$ **do**
32: **if** $deg_{M_l}(i) == \alpha_l$ **then**
33: $d_{h_l} \leftarrow \{d_{h_l}\} \cup \{i\}$
34: **end if**
35: **if** $deg_{M_l}(i) < \alpha_l$ **then**
36: $\widetilde{M}_l \leftarrow \widetilde{M}_l \cup \{i\}$
37: **end if**
38: **end for**
39: **for all** $k \in d_{h_l}$ **do**
40: $\mathcal{E}_H \leftarrow \mathcal{E}_H \cup \{(k,h_l)\}$
41: **end for**
42: **for all** $k \in \widetilde{M}_l$ **do**
43: **if** $(k,d) \notin \mathcal{E}_R$ for all $d \in d_{h_l}$ **then**
44: $\mathcal{E}_H \leftarrow \mathcal{E}_H \cup \{(k,h_l)\}$
45: **end if**
46: **end for**
47: **end if**
48: **end for**
49: $\mathcal{V}_R \leftarrow \mathcal{V}_H \cup \mathcal{V}_o$
50: $\mathcal{E}_R \leftarrow \mathcal{E}_H \cup \mathcal{E}_R$
51: Return $\mathcal{V}_R$, $\mathcal{E}_R$

0018-9286 (c) 2021 IEEE. Personal use is permitted, but republication/redistribution requires IEEE permission. See http://www.ieee.org/publications_standards/publications/rights/index.html for more information.
Authorized licensed use limited to: University of Minnesota. Downloaded on August 12,2022 at 21:08:33 UTC from IEEE Xplore. Restrictions apply.

This article has been accepted for publication in a future issue of this journal, but has not been fully edited. Content may change prior to final publication. Citation information: DOI 10.1109/TAC.2021.3124979, IEEE Transactions on Automatic Control

is applicable to networks with or without latent nodes.

VI. IPSD Estimation from Finite time-series

In this section, we investigate the effect of finite time-series on the estimation of the IPSDM. Suppose that we are given the time-series $\{\mathbf{x}(t) \in \mathbb{R}^n\}_{t=1}^N$. We show that, with high probability, the entries of an estimated IPSDM are close to the original IPSDM, if the number of samples, N is large enough. To begin with, recall that (13) can be rewritten as $\widetilde{\mathbf{x}}(t) = \sum_{k=-\infty}^{\infty} \widetilde{\xi}(k)\widetilde{\boldsymbol{e}}(t-k),\ t \in \mathbb{Z}$, where $\xi(z) := (\mathbf{I} - \mathbf{H}(z))^{-1}$. Similar to [47], for the convenience of analysis, we define:

$$\mathcal{H}_\rho(l, L) := \{(\mathbf{x}(t), t \in \mathbb{Z}) : 0 < l \leqslant |\lambda(\xi(z))| \leqslant L, \text{for } |z| \leqslant \rho\}, \quad (23)$$

where $\lambda(\xi(z))$ denotes eigenvalues of $\xi(z)$, and restrict ourselves to the family $\mathcal{H}_\rho(l, L)$.

A. Estimation Error

Here, we characterize the difference between the actual PSDM, $\Phi_{\mathbf{x}}(z)$, in (15) and a PSDM estimated from finite time-series. We assume that the true correlation function $R_{\mathbf{x}}(k) = \mathbb{E}[\widetilde{\mathbf{x}}(0)\widetilde{\mathbf{x}}^T(k)]$ follows the relation

$$\|R_{\mathbf{x}}(k)\|_\infty \leqslant C_1 \rho^{-k}, \quad (24)$$

for some ρ such that $|\rho| < 1$ (recall that $\widetilde{\mathbf{x}}$ is WSS). Note that this assumption is common in scalar Gaussian processes and is an example of strongly mixing process (see [47] and the references therein for details).

Let $\bar{\Phi}_{\mathbf{x}}(z)$ denote the truncated version of the PSDM, $\Phi_{\mathbf{x}}(z)$, and let $\widehat{\Phi}_{\mathbf{x}}(z)$ be the PSDM estimated from data. That is, $\bar{\Phi}_{\mathbf{x}}(z) = \sum_{k=-p}^{p} R_{\mathbf{x}}(k) z^{-k}$, and $\widehat{\Phi}_{\mathbf{x}}(z) = \sum_{k=-p}^{p} \widehat{R}_{\mathbf{x}}(k) z^{-k}$, where $\widehat{R}_{\mathbf{x}}(k) = \frac{1}{N-k}\sum_{l=1}^{N-k} \mathbf{x}(l)\mathbf{x}^T(l+k)$ is the estimated correlation matrix. We employ a concentration bound for $\|\Phi_{\mathbf{x}}(z) - \widehat{\Phi}_{\mathbf{x}}(z)\|_\infty$ to bound $\|\Phi_{\mathbf{x}}^{-1}(z) - \widehat{\Phi}_{\mathbf{x}}^{-1}(z)\|_\infty$, for any $|z| = 1$. By triangle inequality,

$$\begin{aligned}\|\Phi_{\mathbf{x}}(z) - \widehat{\Phi}_{\mathbf{x}}(z)\|_\infty \\ \leqslant \|\Phi_{\mathbf{x}}(z) - \bar{\Phi}_{\mathbf{x}}(z)\|_\infty + \|\bar{\Phi}_{\mathbf{x}}(z) - \widehat{\Phi}_{\mathbf{x}}(z)\|_\infty. \quad (25)\end{aligned}$$

$\|\Phi_{\mathbf{x}}(z) - \bar{\Phi}_{\mathbf{x}}(z)\|_\infty$ is the truncation error, which is the error in truncating PSDM to order p, and $\|\bar{\Phi}_{\mathbf{x}}(z) - \widehat{\Phi}_{\mathbf{x}}(z)\|_\infty$ is the estimation error, which denotes the error in estimating the p-th order truncated PSDM.

The following proposition provides a bound on element-wise distance between $\bar{\Phi}_{\mathbf{x}}$ and $\Phi_{\mathbf{x}}$.

Proposition 5: Consider a linear dynamic system governed by (13). Suppose that the autocorrelation function $R_{\mathbf{x}}(k)$ satisfies (24). For any $\varepsilon > 0$, if $p \geqslant \log_\rho\left(\frac{(1-\rho)\varepsilon}{2C_1}\right) - 1$, then the truncation error $\|\Phi_{\mathbf{x}}(z) - \bar{\Phi}_{\mathbf{x}}(z)\|_\infty \leqslant \varepsilon$.

Proof: See supplementary material, Appendix D or [43]. ■

Note that

$$\begin{aligned}\|\bar{\Phi}_{\mathbf{x}}(z) - \widehat{\Phi}_{\mathbf{x}}(z)\|_\infty &= \left\| \sum_{k=-p}^{p} \left[R_{\mathbf{x}}(k) - \widehat{R}_{\mathbf{x}}(k)\right] z^{-k} \right\|_\infty \\ &\leqslant \sum_{k=-p}^{p} \|R_{\mathbf{x}}(k) - \widehat{R}_{\mathbf{x}}(k)\|_\infty. \quad (26)\end{aligned}$$

Thus, by obtaining a bound on $\|R_{\mathbf{x}}(k) - \widehat{R}_{\mathbf{x}}(k)\|_\infty$, we can upper bound $\|\bar{\Phi}_{\mathbf{x}}(z) - \widehat{\Phi}_{\mathbf{x}}(z)\|_\infty$.

Next, we provide probably approximately correct (PAC) bounds for estimating auto-correlation matrices, which in turn is used in obtaining PAC bounds on PSDMs. The following proposition bounds deviation of each individual elements of auto-correlation matrix.

Proposition 6: For every delay index $k \leqslant N - n$, $k \in \{0, \ldots, p\}$, and all $\varepsilon > 0$, we have

$$\begin{aligned}&\mathbb{P}\left(\|\widehat{R}_{\mathbf{x}}(k) - R_{\mathbf{x}}(k)\|_\infty > \varepsilon\right) \\ &\quad\leqslant n^2 \exp\left(-(N-k)\min\left\{\frac{\varepsilon^2}{32n^2C_1^2}, \frac{\varepsilon}{8nC_1}\right\}\right). \quad (27)\end{aligned}$$

Proof: See supplementary material, Appendix E or [43]. ■

Now, we are ready to obtain the following lemma, which bounds the estimation error in (25) using (26).

Lemma 7: For every $z = e^{j\omega},\ \omega \in (-\pi, \pi]$, the error in estimating truncated PSDM $\widehat{\Phi}_{\mathbf{x}}(z)$ is $\|\bar{\Phi}_{\mathbf{x}}(z) - \widehat{\Phi}_{\mathbf{x}}(z)\|_\infty \leqslant \varepsilon$ with probability at least

$$1 - n^2 \exp\left(-(N-p)\min\left\{\frac{\varepsilon^2}{32(2p+1)^2n^2C_1^2}, \frac{\varepsilon}{8(2p+1)nC_1}\right\}\right).$$

Proof: See supplementary material, Appendix F or [43]. ■

By combining the above lemmas, we obtain the following theorem.

Theorem 6: Consider a linear dynamic system governed by (13). Suppose that the autocorrelation function $R_{\mathbf{x}}(k)$ satisfies (24). Let $0 < \varepsilon_1 < \varepsilon$. Then, for any p such that $p \geqslant \log_\rho\left(\frac{(1-\rho)(\varepsilon-\varepsilon_1)}{2C_1}\right)$, we have $\|\Phi_{\mathbf{x}}(z) - \widehat{\Phi}_{\mathbf{x}}(z)\|_\infty \leqslant \varepsilon$, with probability at least

$$1 - n^2 \exp\left(-(N-p)\min\left\{\frac{\varepsilon_1^2}{32(2p+1)^2n^2C_1^2}, \frac{\varepsilon_1}{8(2p+1)nC_1}\right\}\right).$$

Proof: The proof follows by combining Lemma 7 and Proposition 5. ■

B. IPSDM Estimation Error

Next, we provide a bound for the difference between the original and the estimated IPSDMs in terms of the difference between corresponding PSDMs.

Theorem 7: Consider a linear dynamic system governed by (13) satisfying the Assumption (23). Suppose that the autocorrelation function $R_{\mathbf{x}}(k)$ satisfies (24). Let $0 < \varepsilon_1 < \varepsilon$. Then, for any p such that $p \geqslant \log_\rho\left(\frac{(1-\rho)(\varepsilon-\varepsilon_1)}{2C_1}\right) - 1$, we have

$$\|\Phi_{\mathbf{x}}^{-1} - \widehat{\Phi}_{\mathbf{x}}^{-1}\|_\infty \leqslant \frac{\sqrt{n}L^2\sigma_{e_{[1]}}^2}{l^4\sigma_{e_{[n_o]}}^4}\left(\frac{\sqrt{n}\varepsilon}{l^2\sigma_{e_{[n_o]}}^2 - \sqrt{n}\varepsilon}\right) \quad (28)$$

with probability at least

$$1 - n^2 \exp\left(-(N-p)\min\left\{\frac{\varepsilon_1^2}{32(2p+1)^2n^2C_1^2}, \frac{\varepsilon_1}{8(2p+1)nC_1}\right\}\right),$$

where $\sigma_{e_{[1]}}$ and $\sigma_{e_{[n_o]}}$ denote the largest and the smallest eigenvalues of $\Phi_e(z)$ respectively.

Proof: See supplementary material, Appendix G or [43]. ■

It follows from Theorem 7 that the element-wise distance between $\Phi_{\mathbf{x}}^{-1}$ and $\widehat{\Phi}_{\mathbf{x}}^{-1}$ can be made arbitrarily small with high probability, by picking N large enough.

0018-9286 (c) 2021 IEEE. Personal use is permitted, but republication/redistribution requires IEEE permission. See http://www.ieee.org/publications_standards/publications/rights/index.html for more information.
Authorized licensed use limited to: University of Minnesota. Downloaded on August 12,2022 at 21:08:33 UTC from IEEE Xplore. Restrictions apply.

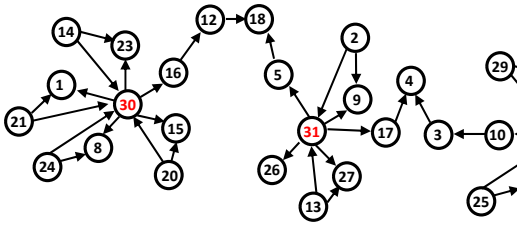

Fig. 2: LDG $\mathcal{G}(\mathcal{V},\mathcal{E})$ with hidden nodes show

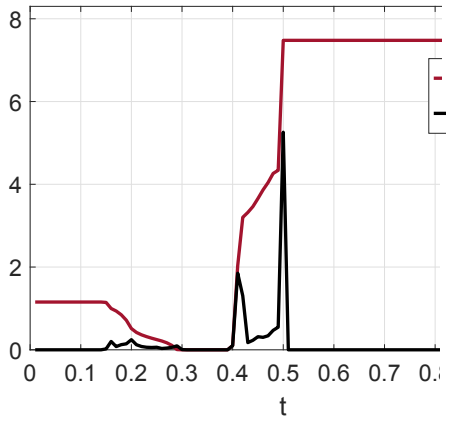

Fig. 3: Comparison between tol_t and $diff_t$ fo decomposition of $\Im\{\Phi_{oo}^{-1}\}$ obtained by the LD

VII. Simulation results

In this section, we validate our algorithms tions. All the simulations are performed in Ma the optimization problem for matrix decompos YALMIP [48] with SDPT3 [49] solver.

For the simulations, we assume that we have access to the perfect IPSDM, Φ_{oo}^{-1}. From $\Im\{\Phi_{oo}\}$ alone, we aim to reconstruct the topology of the LDM which involves (a) recover the topology restricted to observed nodes given by $\mathcal{T}(\mathcal{V}_o,\mathcal{E}_o)$, (b) determine the number of hidden nodes n_h in LDG $\mathcal{G}(\mathcal{V},\mathcal{E})$, and (c) reconstruct topology associated with each hidden node.

Remark 21: The objective of our simulation is to demonstrate the working of Algorithm 1 to decompose $\Im\{\Phi_{oo}^{-1}\}$ of this network into $\widehat{\mathbf{S}} = \Im\{\mathbf{S}\}$ and $\widehat{\mathbf{L}} = \Im\{\mathbf{L}\}$. Then, by applying algorithms 2 and 3 on $\widehat{\mathbf{S}}$ and $\widehat{\mathbf{L}}$, we can retrieve the original topology.

A. LDM

For the simulation, we assume that Φ_{oo} of a topologically detectable LDM in (17) with 32 nodes, having the LDG as shown in Fig. 2 is given. The nodes colored in red $(30, 31, 32)$ are hidden and the rest are observed. Note that the network in Fig. 2 and the corresponding LDM satisfies the assumptions 1-5.

B. Sparse plus low-rank decomposition of $\Im\{\Phi_{oo}^{-1}(z)\}$

We applied Algorithm 1 for matrix decomposition of $\Im\{\Phi_{oo}^{-1}(z)\}$ to obtain $\Im\{\mathbf{S}(z)\} = \hat{\mathbf{S}}$ and $\Im\{\mathbf{L}(z)\} = \hat{\mathbf{L}}$. Here, we took $z = e^{j\frac{3\pi}{8}}$ and $\epsilon = 0.01$ for running Algorithm 1. Fig. 3 shows the values of tol_t and $diff_t$ corresponding

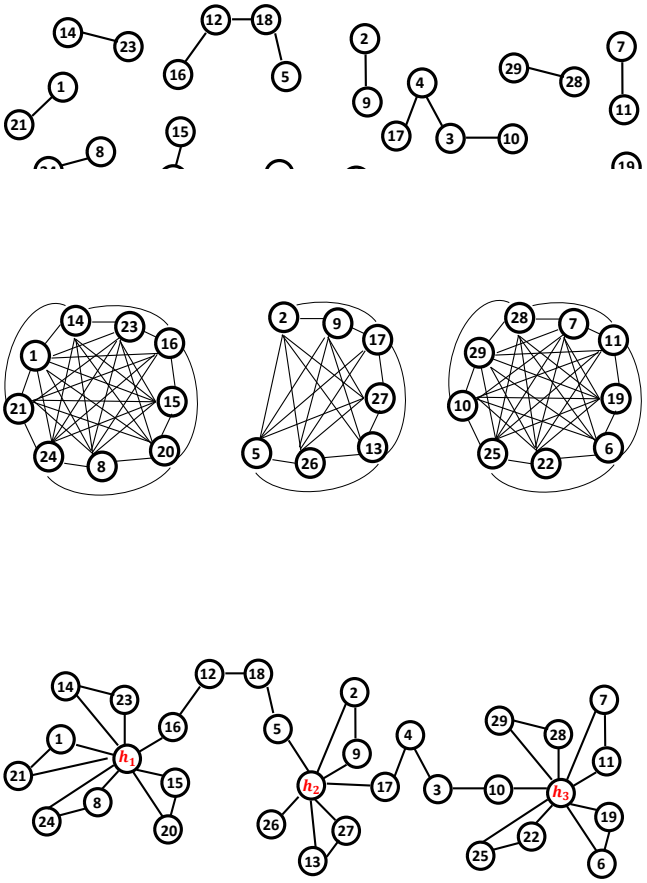

Fig. 5: $\mathcal{T}(\mathcal{V}_R,\mathcal{E}_R)$: Final reconstructed topology with hidden nodes.

to the decomposition of $\Im\{\Phi_{oo}^{-1}(z)\}$ for various values of t. From the plots, we see that the $diff_t$ plot shows three zero regions, similar to what was proposed in Proposition 3. We would like to stress that the network does not satisfy the sufficient condition of Lemma 4. Nevertheless, the plot can retrieve the true sparse and low-rank matrices by picking a t in the middle zero region, as described by Algorithm 2. This network belongs to the subclass of the networks that does not satisfy the sufficient condition of Lemma 4, but satisfy the necessary and sufficient condition of (7).

We make three important observations in Fig. 3: (a) for small t, we observe a beginning zero region where $diff_t$ is zero. This verifies Proposition 3: when the value of t is very small (smaller than 0.15), the optimal objective value is obtained by setting zero to $\Im\{\mathbf{L}\}$ and the objective achieves the minimum value of zero at $(\Im\{\mathbf{S}\} + \Im\{\mathbf{L}\}, 0)$. As t is increased but less than 0.15, we still obtain the optimal solution at $(\Im\{\mathbf{S}\} + \Im\{\mathbf{L}\}, 0)$, and hence, $diff_t$ is zero for t very small. (b) The opposite behavior is observed when t is very large (greater than 0.5). This is the end zero region, which corresponds to the optimal solution at $(0, \Im\{\mathbf{S}\} + \Im\{\mathbf{L}\})$. Nevertheless, the value of tol_t is quite high for both of these scenarios, since neither of the solutions are correct. (c) In the middle region ($t \in [0.24, 0.35]$) , it is observed that both the tol_t and $diff_t$ are zero; the range

0018-9286 (c) 2021 IEEE. Personal use is permitted, but republication/redistribution requires IEEE permission. See http://www.ieee.org/publications_standards/publications/rights/index.html for more information.
Authorized licensed use limited to: University of Minnesota. Downloaded on August 12,2022 at 21:08:33 UTC from IEEE Xplore. Restrictions apply.

This article has been accepted for publication in a future issue of this journal, but has not been fully edited. Content may change prior to final publication. Citation information: DOI 10.1109/TAC.2021.3124979, IEEE Transactions on Automatic Control

specified by Proposition 2 (See Corollary 1).

Note that $diff_t$ need not be zero in the middle region. However, it is observed from simulations that if we pick a t corresponding to minimum value of $diff_t$ in the middle region between $(0.3, 0.4)$, it is still possible to reconstruct topology. This is because the finite value of $diff_t$ in middle region is due to element wise mismatch of non-zero entries. However, the structural pattern of sparse and low-rank matrices is almost preserved. For topology reconstruction, structural pattern is more important than the exactness of the element wise values.

C. Reconstruction of $\mathcal{T}(\mathcal{V}, \mathcal{E})$

Topology reconstruction of the LDM involves (a) recover the topology restricted to observed nodes given by $\mathcal{T}(\mathcal{V}_o, \mathcal{E}_o)$, (b) determine the number of hidden nodes n_h in LDG $\mathcal{G}(\mathcal{V}, \mathcal{E})$ and (c) reconstruct the topology associated with each hidden node.

From Fig. 3, it is evident that $\Im\{\Phi_{oo}^{-1}(z)\}$ was decomposed uniquely into $\Im\{\mathbf{S}\}$ and $\Im\{\mathbf{L}\}$ when $t \in [0.3, 0.4]$, since tol_t is zero. Indeed, due to perfect retrieval, the optimal solution is $(\Im\{\mathbf{S}\}, \Im\{\mathbf{L}\})$. We now use the decomposed matrices $\Im\{\mathbf{S}\}$ and $\Im\{\mathbf{L}\}$ with $\tau = 10^{-6}$ to obtain the following:

(a) From $\Im\{\mathbf{S}\}$, we apply Algorithm 2 to obtain the topology of the subgraph restricted to the observable nodes. The reconstructed topology among observed nodes is shown in Fig. 4a, which matches perfectly with topology of the LDG in Fig. 2 restricted to observed nodes $\mathcal{T}(\mathcal{V}_o, \mathcal{E}_o)$.

(b) From $\Im\{\mathbf{L}\}$, we apply Algorithm 3 and construct (V_H, E_H), which is a union of three disjoint connected subgraphs, i.e., $(V_H, E_H) = \bigcup_{l=1}^{3} (M_l, Q_l)$ (refer Fig. 4b). Therefore, number of hidden nodes in the LDG are three hidden nodes present. n_h is 3.

(c) In Fig. 4b, each connected component (M_l, Q_l) is a clique. For $l = \{1, 2, 3\}$, Algorithm 3 considers l^{th} clique (M_l, Q_l), places a single hidden node h_l in the clique and reconstructs the topology associated with hidden node h_l. Since (M_l, Q_l) is a clique, $M_l = \mathcal{C}(h_l) \cup \{\mathcal{P}(h_l) \cap \mathcal{S}(h_l)\}$.

From (a), (b), and (c), Algorithm 3 reconstructs the complete topology including latent nodes (see Fig. 5), which matches exactly with the topology of the LDG. To summarize, Algorithm 1 decomposed $\Im\{\Phi_{oo}^{-1}(z)\}$ into sum of sparse $\Im\{\mathbf{S}\}$ and low-rank $\Im\{\mathbf{L}\}$. Using $\Im\{\mathbf{S}\}$, Algorithm 2 reconstructs the topology reconstructed to observable nodes. Using $\Im\{\mathbf{L}\}$, Algorithm 3 estimates the number of hidden nodes, reconstructs the topology associated with each hidden node and the full topology of the LDG in Fig. 2 is reconstructed as shown in Fig. 5, which matched exactly with true topology of the LDG.

VIII. Conclusions

We presented a novel approach to reconstruct the topology of networked linear dynamical systems with latent agents, from IPSDM of the observed nodes. The network was allowed to have directed loops and bi-directed edges. It was shown that the IPSDM can be uniquely decomposed into a sparse and a low-rank matrices. The sparse component unveiled the moral graph of the observed nodes, and the low-rank component retrieved the Markov Blanket associated with the latent nodes. Necessary and sufficient conditions for unique sparse plus low-rank decomposition of a skew symmetric matrix was established, along with an optimization based algorithm that decompose the skew symmetric matrix to yield the sparse component $\mathbf{S}$ and the low-rank component $\mathbf{L}$. For a large class of systems, the unique decomposition of imaginary part of the IPSDM is sufficient to achieve the moral graph of the observed nodes including the Markov Blanket of latent nodes. Under some assumptions, it was shown that the imaginary part of the IPSDM can be employed to reconstruct the exact topology of the network. Furthermore, concentration bounds on IPSDM estimation from finite time-series is provided.

Appendix

A. Proof of Lemma 1

We show the result for an $n = 3$ skew symmetric matrix. It is straight forward to extend this to a general n. Let $\mathbf{A} = \begin{bmatrix} 0 & a & b \\ -a & 0 & 0 \\ -b & 0 & 0 \end{bmatrix}$ be a skew symmetric matrix. $\mathbf{A}$ can defined as a point on the variety of skew symmetric matrices with support at most 4, i.e., $\mathcal{S}(4) = \mathbb{V}(\mathbf{X}_{11}, \mathbf{X}_{22}, \mathbf{X}_{33}, \mathbf{X}_{12}, \mathbf{X}_{12} + \mathbf{X}_{21}, \mathbf{X}_{13} + \mathbf{X}_{31}, \mathbf{X}_{23} + \mathbf{X}_{32}) \cup \mathbb{V}(\mathbf{X}_{11}, \mathbf{X}_{22}, \mathbf{X}_{33}, \mathbf{X}_{13}, \mathbf{X}_{12} + \mathbf{X}_{21}, \mathbf{X}_{13} + \mathbf{X}_{31}, \mathbf{X}_{23} + \mathbf{X}_{32}) \cup \mathbb{V}(\mathbf{X}_{11}, \mathbf{X}_{22}, \mathbf{X}_{33}, \mathbf{X}_{23}, \mathbf{X}_{12} + \mathbf{X}_{21}, \mathbf{X}_{13} + \mathbf{X}_{31}, \mathbf{X}_{23} + \mathbf{X}_{32})$.

Define $f_{ii} := \mathbf{X}_{ii}, \forall 1 \leqslant i \leqslant n$, $f_{ij} := \mathbf{X}_{ij} + \mathbf{X}_{ji}, \forall 1 \leqslant i < j \leqslant n$, and $g_{ij} := \mathbf{X}_{ij}, \forall 1 \leqslant i, j \leqslant n$. Note that $\mathbf{A}$ is a point on the variety defined by $f_{ii} = 0$, $1 \leqslant i \leqslant n$, $f_{12} = 0$, $f_{13} = 0$, $f_{23} = 0$, and $g_{23} = 0$, and is non-singular point (with respect to the variety). The tangent space of $\mathcal{S}(4)$ at $\mathbf{A}$, $T(\mathbf{A})$, is (see Proposition 9.6.2 in [41]):

$$T(\mathbf{A}) = \mathbb{V}\left((d_{\mathbf{A}}(f_{ii}))_{i=1}^{3}, d_{\mathbf{A}}(f_{12}), d_{\mathbf{A}}(f_{13}), d_{\mathbf{A}}(f_{23}), d_{\mathbf{A}}(g_{23}) \right), \quad (29)$$

where $d_{\mathbf{A}}(f) := \sum_{i,j=1}^{3} \frac{\partial f}{\partial x_{ij}}(\mathbf{A})(\mathbf{X}_{ij} - \mathbf{A}_{ij})$. It can be shown that $d_{\mathbf{A}}(f_{ii}) = \mathbf{X}_{ii}, \forall 1 \leqslant i \leqslant 3$, $d_{\mathbf{A}}(f_{ij}) = \mathbf{X}_{ij} + \mathbf{X}_{ji}, \forall 1 \leqslant i < j \leqslant 3$, and $d_{\mathbf{A}}(g_{23}) = \mathbf{X}_{23}$. Plugging this in (29), we obtain

$$T(\mathbf{A}) = \left\{ \begin{bmatrix} 0 & \mathbf{X}_{12} & \mathbf{X}_{13} \\ -\mathbf{X}_{12} & 0 & 0 \\ -\mathbf{X}_{13} & 0 & 0 \end{bmatrix} : \mathbf{X}_{12}, \mathbf{X}_{13} \in \mathbb{R} \right\}. \quad (30)$$

Clearly, this is the space of all skew symmetric matrices with support subset of support of $\mathbf{A}$. Extending this analysis to general n at any point $\mathbf{A}$ gives us the result.

B. Proof of Lemma 2

The following lemma is useful in proving this.

Lemma 8: If $\mathbf{M}$ is a skew symmetric $n \times n$ matrix of rank r (r even or $n > r$ odd), then there exists a non-singular matrix $\mathbf{P}$ such that $\mathbf{M} = \mathbf{P}\mathbf{Q}\mathbf{P}^T$, where $\mathbf{Q} = \begin{bmatrix} \mathbf{J} & \mathbf{0} \\ \mathbf{0} & \mathbf{0} \end{bmatrix}$ and $\mathbf{J} = diag\left(\begin{bmatrix} 0 & 1 \\ -1 & 0 \end{bmatrix}, \begin{bmatrix} 0 & 1 \\ -1 & 0 \end{bmatrix}, \ldots, \begin{bmatrix} 0 & 0 \\ 0 & 0 \end{bmatrix} \right)$.

Let $\mathcal{R}(r) := \{\mathbf{X} \in \mathbb{R}^{n \times n} : rank(\mathbf{X}) = r, \ \mathbf{X} + \mathbf{X}^T = 0\}$ be the space of skew symmetric matrices with rank r. By Youla decomposition (Lemma 8), this is equivalent to $\mathcal{R}(r) = \{\mathbf{P}\mathbf{Q}\mathbf{P}^T : \mathbf{P} \in \mathbb{R}^{n \times n} \text{ invertible}\}$.

0018-9286 (c) 2021 IEEE. Personal use is permitted, but republication/redistribution requires IEEE permission. See http://www.ieee.org/publications_standards/publications/rights/index.html for more information.
Authorized licensed use limited to: University of Minnesota. Downloaded on August 12,2022 at 21:08:33 UTC from IEEE Xplore. Restrictions apply.

This article has been accepted for publication in a future issue of this journal, but has not been fully edited. Content may change prior to final publication. Citation information: DOI 10.1109/TAC.2021.3124979, IEEE Transactions on Automatic Control

As shown in [42], $\mathcal{R}(r)$ is a smooth manifold. Let $\mathbf{M}$ be an element in $\mathcal{R}(r)$. Let $\boldsymbol{\gamma} : (-1,1) \rightarrow \mathcal{R}(r)$ be a smooth map such that $\boldsymbol{\gamma}(t) = \mathbf{P}(t)\mathbf{Q}\mathbf{P}^T(t)$ with $\boldsymbol{\gamma}(0) = \mathbf{P}(0)\mathbf{Q}\mathbf{P}^T(0) = \mathbf{M}$, where $\mathbf{P}(t)$ is invertible . Then, $\frac{d\boldsymbol{\gamma}(t)}{dt} = \frac{d\mathbf{P}(t)}{dt}\mathbf{Q}\mathbf{P}^T(t) + \mathbf{P}(t)\mathbf{Q}\frac{d\mathbf{P}^T(t)}{dt}$. For $t = 0$, this can be written as $\frac{d\boldsymbol{\gamma}(t)}{dt}\Big|_{t=0} = \Delta\mathbf{M} + \mathbf{M}\Delta^T$, where $\Delta = \frac{d\mathbf{P}}{dt}(0)\mathbf{P}^{-1}(0)$. Define $W := \{\Delta\mathbf{M} + \mathbf{M}\Delta^T : \Delta \in \mathbb{R}^{n\times n}\}$ and let $\Gamma_M := \{\boldsymbol{\gamma}'(0) : \boldsymbol{\gamma}$ is a smooth map from (-1,1) to $\mathcal{R}(r)\}$ be the tangent space with respect to $\mathcal{R}(r)$ at $\mathbf{M}$. We claim that $\Gamma_M = W$. $\Gamma_M \subseteq W$ is obvious. To show the converse, let $w \in W$. Let Δ be such that $\Delta\mathbf{M} + \mathbf{M}\Delta^T = w$, and choose $\mathbf{P}(t) := \mathbf{P}(0) + t\Delta\mathbf{P}(0)$. Invertibility of $\mathbf{P}(t)$ follows from invertibility of $\mathbf{P}(0)$ and continuity of determinant. We need to show that this map belongs to the tangent space Γ_M. Note that $\frac{d\mathbf{P}(t)}{dt}\Big|_{t=0} = \Delta\mathbf{P}(0)$ and $\frac{d\boldsymbol{\gamma}(t)}{dt}\Big|_{t=0} = \Delta\mathbf{M} + \mathbf{M}\Delta^T$, which proves the claim. Plugging in $\mathbf{M}^T = -\mathbf{M}$ and CSVD, $\mathbf{M} = \mathbf{U}\Sigma\mathbf{Q}\mathbf{U}^T$, in the definition of W, and substituting $\mathbf{X} = -\Delta\mathbf{U}\Sigma\mathbf{Q}$ completes the proof.

C. Proof of Proposition 3

For any matrix $\mathbf{A} \in \mathbb{R}^{n\times n}$, $\frac{1}{k_1}\|\mathbf{A}\|_1 \leqslant \|\mathbf{A}\|_* \leqslant k_2\|\mathbf{A}\|_1$, where k_1, k_2 are real numbers. Note that k_1 and k_2 can be functions of n. The tightest bound available is $k_1 = n$ and $k_2 = 1$ [45].

Define $f(\mathbf{S},\mathbf{L},t) := t\|\mathbf{S}\|_1 + (1-t)\|\mathbf{L}\|_*$. Clearly, the minimum value at $t = 0$ is $f(\widehat{\mathbf{S}}_0, \widehat{\mathbf{L}}_0, \mathbf{0}) = 0$, and is obtained at the point $(\widehat{\mathbf{S}}, \widehat{\mathbf{L}}) = (\mathbf{C}, \mathbf{0})$. Next, consider $t = \epsilon$ for some ϵ close to zero. The objective value at $(\mathbf{S},\mathbf{L}) = (\mathbf{C}-\mathbf{N}, \mathbf{N})$ for $t = \epsilon$, where $\mathbf{N} \neq \mathbf{0}$ is

$$f(\mathbf{S},\mathbf{L},\epsilon) = \epsilon\|\mathbf{C}-\mathbf{N}\|_1 + (1-\epsilon)\|\mathbf{N}\|_*. \tag{31}$$

Let the objective value for $t = \epsilon$ at the point $(\mathbf{C},\mathbf{0})$ be $g(\epsilon) := f(\mathbf{C},\mathbf{0},\epsilon) = \epsilon\|\mathbf{C}\|_1$. This can be rewritten as

$$\begin{aligned} g(\epsilon) &= \epsilon\|\mathbf{C}-\mathbf{N}+\mathbf{N}\|_1 \leqslant \epsilon\|\mathbf{C}-\mathbf{N}\|_1 + \epsilon\|\mathbf{N}\|_1 \\ &\leqslant \epsilon\|\mathbf{C}-\mathbf{N}\|_1 + \epsilon k_1\|\mathbf{N}\|_*, \end{aligned} \tag{32}$$

where the first inequality follows from the triangle inequality, and the second inequality follows since $\|\mathbf{N}\|_1 \leqslant k_1\|\mathbf{N}\|_*$.

Then, $f(\mathbf{S},\mathbf{L},\epsilon) - g(\epsilon) \geqslant (1-(k_1+1)\epsilon)\|\mathbf{N}\|_*$. For $0 < \epsilon < \epsilon_L$, where $\epsilon_L = \frac{1}{k_1+1}$, we have that $f(\mathbf{S},\mathbf{L},\epsilon) - g(\epsilon) > 0$, since $\|\mathbf{N}\|_* > 0$. Thus, we have shown that for $t = \epsilon$ the value of the objective function at $(\mathbf{C}-\mathbf{N},\mathbf{N})$ is strictly greater than that at $(\mathbf{C},\mathbf{0})$. Moreover, this is true for all $\mathbf{N} \neq \mathbf{0}$. Therefore, we can conclude that for $0 \leqslant t < \epsilon_L$, the optimal solution is $(\mathbf{C},\mathbf{0})$.

Similarly, it is easy to see that the minimum value at $t = 1$, $f(\widehat{\mathbf{S}}_1, \widehat{\mathbf{L}}_1, 1) = 0$, and is obtained at the point $(\mathbf{S},\mathbf{L}) = (\mathbf{0},\mathbf{C})$. Proceeding similar to the above analysis for $t = 1$, with $(\mathbf{S},\mathbf{L}) = (\mathbf{N},\mathbf{C}-\mathbf{N})$ and $g(\epsilon) := f(\mathbf{0},\mathbf{C},\epsilon) = (1-\epsilon)\|C\|_*$, we can conclude that $f(\mathbf{S},\mathbf{L},\epsilon) - g(\epsilon) \geqslant (1-(k_2+1)\epsilon)\|\mathbf{N}\|_1$. For $\epsilon_U < t \leqslant 1$, where $\epsilon_U = \frac{k_2}{k_2+1}$, we have that $f(\mathbf{S},\mathbf{L},\epsilon) - g(\epsilon) > 0$, for every $\mathbf{N} \neq \mathbf{0}$. Thus, for $t > \epsilon_U$, the optimal solution is $(\mathbf{0},\mathbf{C})$

Proposition 2 and Lemma 4 showed that (with the change of variable $t = \gamma/(1+\gamma)$), for every t within the specified range, the optimal solution is $(\widehat{\mathbf{S}}_t, \widehat{\mathbf{L}}_t) = (\tilde{\mathbf{S}}, \tilde{\mathbf{L}})$. That is, if $\mu\xi < 1/6$ or $\deg_{\max}(\tilde{\mathbf{S}})inc(\tilde{\mathbf{L}}) < 1/12$, then we can find an interval $(t_1,t_2) \subset [0,1]$ with $0 < t_1 < t_2 < 1$ such that $(\tilde{\mathbf{S}},\tilde{\mathbf{L}}) = (\hat{\mathbf{S}}_t,\hat{\mathbf{L}}_t)$ for any $t \in (t_1,t_2)$. This implies that $diff_t = 0$ for $t \in [t_1+\varepsilon, t_2-\varepsilon]$ and sufficiently small interval ε. Therefore, there exists at least three zero regions for the plot of $diff_t$ versus t if any of the sufficient conditions mentioned above is satisfied and ε is small enough.

D. Proof of Theorem 1

To prove the first part, let $\overline{\mathcal{E}}_o$ be the set of undirected edges obtained by removing direction from $\mathcal{E}_o$, without repetition. Then, by Proposition 4, $\overline{\mathcal{E}}_o \cup \mathcal{E}_o^{ss} \supseteq \{(i,j) : \mathbf{S}_{ij} \neq 0,\ i < j\}$, i.e., $|support(\mathbf{S})| \leqslant 2|\overline{\mathcal{E}}_o| + 2|\mathcal{E}_o^{ss}| + n \leqslant 2|\mathcal{E}_o| + 2|\mathcal{E}_o^{ss}| + n$, where the additional n is due to the diagonal entries of $\mathbf{S}$.

To show the upper bound on rank, let $\mathbf{A} = \Psi^*\Lambda^{-1}\Psi$. Notice that $rank(\mathbf{A}) \leqslant \min\{rank(\Psi), rank(\Lambda)\} \leqslant n_h$. Similarly, $rank(\mathbf{H}_{ho}^*\Phi_{e_h}^{-1}\mathbf{H}_{ho}) \leqslant n_h$. Then, $rank(L) \leqslant 2n_h$ from (20).

E. Proof of Theorem 4

From (19), observe that $\mathbf{S}$ is a Hermitian matrix, which is true if and only if $\Im\{\mathbf{S}\}$ is anti-symmetric, and thus the diagonal entries of $\Im\{\mathbf{S}\}$ are zeros. Lemma 5 showed that if $\mathbf{S}_{ij} \neq 0$, then $(i,j) \in kin(\mathcal{G}_o)$. Combining this with Lemma 6, we get if $\Im(\mathbf{S}_{ij}) \neq 0$ then $i \in \mathcal{C}(j)$ or $i \in \mathcal{P}(j)$. That is, $\hat{\mathcal{E}}_o \subseteq \overline{\mathcal{E}}_o$.

To prove the equality, we need to show that $\hat{\mathcal{E}}_o \supseteq \overline{\mathcal{E}}_o$. Let $i \neq j$ and suppose $[\mathbf{H}_{oo}]_{ij} \neq 0$. By expanding (19), $\mathbf{S}_{ij} = (\Phi_{e_o}^{-1})_{ij} - \sum_{k=1}^n (\mathbf{H}_{oo}^*)_{ik}(\Phi_{e_o}^{-1})_{kj} - \sum_{k=1}^n (\Phi_{e_o}^{-1})_{ik}(\mathbf{H}_{oo})_{kj} + \sum_{k=1}^n\sum_{l=1}^n (\mathbf{H}^*)_{ik}(\Phi_{e_o}^{-1})_{kl}(\mathbf{H}_{oo})_{lj}$. Clearly $\mathbf{S}_{ij} \neq 0$ since $[\mathbf{H}_{oo}]_{ij} \neq 0$, except for a few pathological cases that occur with Lebesgue measure zero. It follows by Assumption 3 that $\Im\{\mathbf{S}_{ij}\} \neq 0$, except over a set of Lebesgue measure zero.

F. Proof of Theorem 2

Recall expression (20) for $\mathbf{L}$. By expanding each term in (20) we obtain that if $\mathbf{H}_{hh} = 0$, then Λ is diagonal, and $\Psi(k_h,j)$ can be written as

$$\begin{aligned} \Psi(k_h,j) &= \mathbf{H}_{oh}^*(j,k_h)\Phi_{e_{o_j}}^{-1} + \mathbf{H}_{ho}(k_h,j)\Phi_{e_{h_{k_h}}}^{-1} \\ &- \sum_{k=1}^{n_o} \Phi_{e_{o_k}}^{-1}\mathbf{H}_{oh}^*(k,k_h)\mathbf{H}_{oo}(k,j) \end{aligned} \tag{33}$$

Then, we can conclude the following from the aforementioned equations.

- If the hidden nodes are at least two hops away, then Λ is real and diagonal.
- If any of $k_h \rightarrow j$ or $j \rightarrow k_h$ or $k_h \rightarrow k \leftarrow j$ exists for some $k \in \mathcal{V}_o$, then $\Psi_{k_h,j} \neq 0$
- For $i \neq j$, $\mathbf{L}_{ij}$ is given by the expression (34) below.

$$\begin{aligned} \mathbf{L}_{i,j} = &\sum_{l=1}^{n_h} [\mathbf{H}_{ho}^*(l,i)]\Phi_{e_{h,l}}^{-1}\mathbf{H}_{ho}(l,j) - \sum_{l=1}^{n_h} d_l \\ &\left[\mathbf{H}_{oh}(i,l)\Phi_{e_{h,l}}^{-1} + [\mathbf{H}_{ho}^*(l,i)]\Phi_{e_{h,l}}^{-1} - \sum_{k=1}^{n_o}\Phi_{e_{o,k}}^{-1}\mathbf{H}_{oh}(k,l)[\mathbf{H}_{oo}^*(k,i)]\right] \\ &\left[\mathbf{H}_{oh}^*(j,l)\Phi_{e_{h,l}}^{-1} + [\mathbf{H}_{ho}(l,j)]\Phi_{e_{h,l}}^{-1} - \sum_{k=1}^{n_o}\Phi_{e_{o,k}}^{-1}\mathbf{H}_{oh}^*(k,l)[\mathbf{H}_{oo}(k,j)]\right] \end{aligned} \tag{34}$$

Let a_1, a_2, and a_3 respectively denote first, second, and third terms in the first bracket and let b_1, b_2, and b_3 respectively

0018-9286 (c) 2021 IEEE. Personal use is permitted, but republication/redistribution requires IEEE permission. See http://www.ieee.org/publications_standards/publications/rights/index.html for more information.
Authorized licensed use limited to: University of Minnesota. Downloaded on August 12,2022 at 21:08:33 UTC from IEEE Xplore. Restrictions apply.

This article has been accepted for publication in a future issue of this journal, but has not been fully edited. Content may change prior to final publication. Citation information: DOI 10.1109/TAC.2021.3124979, IEEE Transactions on Automatic Control

denote first, second, and third terms in the second bracket. Then, (34) can be rewritten as,

$$\begin{aligned}\mathbf{L}(i,j) &= \sum_{l=1}^{n_h}[\mathbf{H}_{ho}(l,i)]^*\Phi_{e_{h,l}}^{-1}\mathbf{H}_{ho}(l,j)- \\ &\quad \sum_{l=1}^{n_h} d_l\left[a_1+a_2+a_3\right]\left[b_1+b_2+b_3\right] \\ &= \sum_{l=1}^{n_h}[\mathbf{H}_{ho}(l,i)]^*\Phi_{e_{h,l}}^{-1}\mathbf{H}_{ho}(l,j)- \\ &\quad -\sum_{l=1}^{n_h} d_l[a_1b_1+a_1b_2+a_1b_3+a_2b_1+a_2b_2+ \\ &\qquad a_2b_3+a_3b_1+a_3b_2+a_3b_3]. \end{aligned} \tag{35}$$

(a) We use contrapositive argument to prove this. Suppose that, for every hidden node $h \in \mathcal{V}_h$, there does not exist $g \in DM_h(i,j)$ such that $g \in \mathcal{G}(\mathcal{V},\mathcal{E})$. Then, from (35), it follows that $\mathbf{L}_{ij} = 0$. Therefore, if $\mathbf{L}_{ij} \neq 0$, then there exists $g \in DM_h(i,j)$ such that $g \in \mathcal{G}(\mathcal{V},\mathcal{E})$, for some $h \in \mathcal{V}_h$. Clearly, for any $g \in DM_h(i,j)$, we have $d_{hop}(i,h) \leqslant 2$ and $d_{hop}(j,h) \leqslant 2$.

(b) Let $i,j \in \mathcal{V}_o$. Suppose that $\mathbf{L}_{ij} \neq 0$. Then, from part (a), there exists $g_1 \in DM_{h_1}(i,j)$ such that $g_1 \in \mathcal{G}(\mathcal{V},\mathcal{E})$, for some $h_1 \in \mathcal{V}_h$. Suppose for contradiction that there exists $h_2 \in \mathcal{V}_h\backslash\{h_1\}$ such that there exists $g_2 \in DM_{h_2}(i,j)$ such that $g_2 \in \mathcal{G}(\mathcal{V},\mathcal{E})$. Then, we have $d_{hop}(h_1,h_2) \leqslant d_{hop}(h_1,i)+d_{hop}(i,h_2) \leqslant 4$ from Theorem 2(a), which contradicts Assumption 2. Hence, $h_1 = h_2$.

G. Proof of Theorem 3

(a) Suppose $M_{l_1} \cap M_{l_2} \neq \varnothing$ for some $l_1,l_2 \in \mathcal{V}_h, l_1 \neq l_2$. Then, there exists $a \in M_{l_1} \cap M_{l_2}$. Since $a \in M_{l_1}$, it follows from the definition of M_{l_1} that $d_{hop}(a,l_1) \leqslant 2$. Similarly, $a \in M_{l_2}$ and $d_{hop}(a,l_2) \leqslant 2$. Then, we have $d_{hop}(l_1,l_2) \leqslant d_{hop}(l_1,a)+d_{hop}(a,l_2) \leqslant 4$, which contradicts Assumption 2. Therefore, $M_{l_1} \cap M_{l_2} = \varnothing$ for all $l_1,l_2 \in \mathcal{V}_h, l_1 \neq l_2$.

(b) Suppose $Q_{l_1} \cap Q_{l_2} \neq \varnothing$ for some $l_1,l_2 \in \mathcal{V}_h, l_1 \neq l_2$. Then, there exists $(i_0,j_0) \in Q_{l_1} \cap Q_{l_2}$. $(i_0,j_0) \in Q_{l_1}$, which implies that $i_0,j_0 \in M_{l_1}$. Similarly, $(i_0,j_0) \in Q_{l_2}$ implies that $i_0,j_0 \in M_{l_2}$. Thus, $i_0,j_0 \in M_{l_1} \cap M_{l_2}$, which contradicts part (a). Therefore, $Q_{l_1} \cap Q_{l_2} = \varnothing$.

(c) We first show that $V_H \supseteq \bigcup_{l=1}^{n_h} M_l$. To show this, let $a \in \bigcup_{l=1}^{n_h} M_l$. Then, $a \in M_l$ for some $l \in \mathcal{V}_h$. It follows from the definition of M_l that $a \in \mathcal{P}(l) \cup \mathcal{C}(l) \cup \mathcal{S}(l)$. If $a \in \mathcal{P}(l) \cup \mathcal{C}(l)$, then by Assumption 1, there exists $c \in M_l\backslash a$. If $a \in \mathcal{S}(l)\backslash(\mathcal{C}(l) \cup \mathcal{P}(l))$, then there exists $k \in M_l\backslash a$, such that $k \in \mathcal{C}(l) \cap \mathcal{C}(a)$. Given the existence of node $k \in \mathcal{C}(l)$, by Assumption 1 there exists $c \in M_l\backslash\{a,k\}$. Clearly there is a node $c \in M_l\backslash a$ in $\mathcal{G}(\mathcal{V},\mathcal{E})$, which is also present in $DM_l(a,c)$. From (35) and Remark 13, it follows that $\mathbf{L}_{ac} \neq 0$. Because $\mathbf{L}_{ac} \neq 0$, it follows from the definition V_H, that $a \in V_H$. Now, we show that $V_H \subseteq \bigcup_{l=1}^{n_h} M_l$. Let $a \in V_H$, then from the definition of V_H, there exists $c \in \mathcal{V}_o\backslash a$, such that $\mathbf{L}_{ac} \neq 0$. From Theorem 2 parts (a) and (b), there exists a unique hidden node $l \in \mathcal{V}_h$ such that $g \in DM_l(a,k)$ exists in $\mathcal{G}(\mathcal{V},\mathcal{E})$. From the definition of $DM_l(a,k)$, it follows that $a \in M_l$. Hence, $a \in \bigcup_{l=1}^{n_h} M_l$, which concludes the proof.

We first show $E_H \supseteq \bigcup_{l=1}^{n_h} Q_l$. Let $(i_0,j_0) \in \bigcup_{l=1}^{n_h} Q_l$, then there exists a $l \in \mathcal{V}_h$, such that $(i_0,j_0) \in Q_l$. From the definition of $Q_l, \{i_0,j_0\} \in M_l \subset V_H$ and $\mathbf{L}_{i_0j_0} \neq 0$. Thus $(i_0,j_0) \in E_H$.

To show the converse $E_H \subseteq \bigcup_{l=1}^{n_h} Q_l$, let $(i_0,j_0) \in E_H$, then $\mathbf{L}_{i_0j_0} \neq 0$. From Theorem 2(b), there exists a unique hidden node $l \in \mathcal{V}_h$, such that a $g \in DM_l(i_0,j_0)$ exists in $\mathcal{G}(\mathcal{V},\mathcal{E})$. It follows from the definition of $DM_l(i_0,j_0)$ that $\{i_0,j_0\} \in M_l$. $\{i_0,j_0\} \in M_l$. and $\mathbf{L}_{i_0j_0} \neq 0$, thus $(i_0,j_0) \in Q_l \subset \bigcup_{l=1}^{n_h} Q_l$.

REFERENCES

[1] Y.-B. He and Z. Geng, "Active learning of causal networks with intervention experiments and optimal designs," in *Journal of Machine Learning Research*, vol. 9, pp. 1096–1101, Nov 2008.

[2] W. Buntine, "A guide to the literature on learning probabilistic networks from data," *IEEE Transactions on Knowledge and Data Engineering*, vol. 8, pp. 195–210, April 1996.

[3] G. Cavraro and V. Kekatos, "Inverter probing for power distribution network topology processing," *IEEE Transactions on Control of Network Systems*, vol. 6, pp. 980–992, Sep. 2019.

[4] E. Ceci, Y. Shen, G. B. Giannakis, and S. Barbarossa, "Graph-based learning under perturbations via total least-squares," *IEEE Transactions on Signal Processing*, pp. 1–1, 2020.

[5] Y. Shen, X. Fu, G. B. Giannakis, and N. D. Sidiropoulos, "Topology identification of directed graphs via joint diagonalization of correlation matrices," *IEEE Transactions on Signal and Information Processing over Networks*, vol. 6, pp. 271–283, 2020.

[6] M. Jordan, *Learning in Graphical Models*. MIT Press, Cambridge, MA, 1999.

[7] A. J. Wood, B. F. Wollenberg, and G. B. Sheblé, *Power generation, operation, and control*. John Wiley & Sons, 2013.

[8] S. Patel, S. Attree, S. Talukdar, M. Prakash, and M. V. Salapaka, "Distributed apportioning in a power network for providing demand response services," in *2017 IEEE International Conference on Smart Grid Communications (SmartGridComm)*, pp. 38–44, IEEE, 2017.

[9] M. Ghil, M. R. Allen, M. D. Dettinger, K. Ide, D. Kondrashov, M. E. Mann, A. W. Robertson, A. Saunders, Y. Tian, F. Varadi, and P. Yiou, "Advanced spectral methods for climatic time series," *Reviews of Geophysics*, vol. 40, no. 1, pp. 3–1–3–41, 2002.

[10] K. Deng, P. Barooah, P. G. Mehta, and S. P. Meyn, "Building thermal model reduction via aggregation of states," in *Proceedings of the 2010 American Control Conference*, pp. 5118–5123, June 2010.

[11] P. M. Van den Hof, A. Dankers, P. S. Heuberger, and X. Bombois, "Identification of dynamic models in complex networks with prediction error methods—basic methods for consistent module estimates," *Automatica*, vol. 49, no. 10, pp. 2994–3006, 2013.

[12] K. R. Ramaswamy and P. M. Vandenhof, "A local direct method for module identification in dynamic networks with correlated noise," *IEEE Transactions on Automatic Control*, pp. 1–1, 2020.

[13] D. Materassi and M. V. Salapaka, "On the problem of reconstructing an unknown topology via locality properties of the wiener filter," *IEEE Transactions on Automatic Control*, vol. 57, pp. 1765–1777, July 2012.

[14] S. Talukdar, D. Deka, H. Doddi, D. Materassi, M. Chertkov, and M. V. Salapaka, "Physics informed topology learning in networks of linear dynamical systems," *Automatica*, vol. 112, p. 108705, 2020.

[15] M. Dimovska and D. Materassi, "Granger-causality meets causal inference in graphical models: Learning networks via non-invasive observations," in *2017 IEEE 56th Annual Conference on Decision and Control (CDC)*, pp. 5268–5273, Dec 2017.

0018-9286 (c) 2021 IEEE. Personal use is permitted, but republication/redistribution requires IEEE permission. See http://www.ieee.org/publications_standards/publications/rights/index.html for more information.
Authorized licensed use limited to: University of Minnesota. Downloaded on August 12,2022 at 21:08:33 UTC from IEEE Xplore. Restrictions apply.

This article has been accepted for publication in a future issue of this journal, but has not been fully edited. Content may change prior to final publication. Citation information: DOI 10.1109/TAC.2021.3124979, IEEE Transactions on Automatic Control

[16] S. Talukdar, D. Deka, S. Attree, D. Materassi, and M. Salapaka, "Learning the exact topology of undirected consensus networks," in *2017 IEEE 56th Annual Conference on Decision and Control (CDC)*, pp. 5784–5789, Dec 2017.

[17] S. Talukdar, D. Deka, M. Chertkov, and M. Salapaka, "Topology learning of radial dynamical systems with latent nodes," in *2018 Annual American Control Conference (ACC)*, pp. 1096–1101, June 2018.

[18] F. Sepehr and D. Materassi, "Blind learning of tree network topologies in the presence of hidden nodes," *IEEE Transactions on Automatic Control*, vol. 65, pp. 1014–1028, March 2020.

[19] F. Sepehr and D. Materassi, "Inferring the structure of polytree networks of dynamic systems with hidden nodes," in *2016 IEEE 55th Conference on Decision and Control (CDC)*, pp. 4618–4623, Dec 2016.

[20] F. Sepehr and D. Materassi, "An algorithm to learn polytree networks with hidden nodes," in *Advances in Neural Information Processing Systems 32*, pp. 15110–15119, Curran Associates, Inc., 2019.

[21] D. Materassi and M. V. Salapaka, "Network reconstruction of dynamical polytrees with unobserved nodes," in *2012 IEEE 51st IEEE Conference on Decision and Control (CDC)*, pp. 4629–4634, 2012.

[22] D. Materassi and M. V. Salapaka, "Identification of network components in presence of unobserved nodes," in *2015 54th IEEE Conference on Decision and Control (CDC)*, pp. 1563–1568, 2015.

[23] D. Materassi and M. V. Salapaka, "Signal selection for estimation and identification in networks of dynamic systems: A graphical model approach," *IEEE Transactions on Automatic Control*, pp. 1–1, 2019.

[24] D.Materassi, G.Innocenti, L.Giarre, and M. V. Salapaka, "Model identification of a network as compressing sensing," *Systems & Control Letters*, vol. 62, pp. 664–672, 2013.

[25] V. R. Subramanian, A. Lamperski, and M. V. Salapaka, "Network topology identification from corrupt data streams," in *2017 IEEE 56th Annual Conference on Decision and Control (CDC)*, pp. 1695–1700, IEEE, 2017.

[26] V. R. Subramanian, A. Lamperski, and M. V. Salapaka, "Inferring directed graphs for networks from corrupt data-streams," in *2018 IEEE Conference on Decision and Control (CDC)*, pp. 4493–4498, IEEE, 2018.

[27] V. R. Subramanian, A. Lamperski, and M. V. Salapaka, "Corruption detection in networks of bi-directional dynamical systems," in *2019 IEEE 58th Conference on Decision and Control (CDC)*, pp. 4545–4550, IEEE, 2019.

[28] M. S. Veedu and M. V. Salapaka, "Topology identification under spatially correlated noise," *arXiv preprint arXiv:2012.04175*, 2020.

[29] M. Zorzi and R. Sepulchre, "Ar identification of latent-variable graphical models," *IEEE Transactions on Automatic Control*, vol. 61, pp. 2327–2340, Sep. 2016.

[30] R. Liégeois, B. Mishra, M. Zorzi, and R. Sepulchre, "Sparse plus low-rank autoregressive identification in neuroimaging time series," in *2015 54th IEEE Conference on Decision and Control (CDC)*, pp. 3965–3970, Dec 2015.

[31] E. Nozari, Y. Zhao, and J. Cortés, "Network identification with latent nodes via autoregressive models," *IEEE Transactions on Control of Network Systems*, vol. 5, pp. 722–736, June 2018.

[32] D. Alpago, M. Zorzi, and A. Ferrante, "Identification of sparse reciprocal graphical models," *IEEE Control Systems Letters*, vol. 2, no. 4, pp. 659–664, 2018.

[33] V. Ciccone, A. Ferrante, and M. Zorzi, "Factor models with real data: A robust estimation of the number of factors," *IEEE Transactions on Automatic Control*, vol. 64, no. 6, pp. 2412–2425, 2019.

[34] V. Ciccone, A. Ferrante, and M. Zorzi, "Learning latent variable dynamic graphical models by confidence sets selection," *IEEE Transactions on Automatic Control*, vol. 65, no. 12, pp. 5130–5143, 2020.

[35] V. Ciccone, A. Ferrante, and M. Zorzi, "Robust identification of "sparse plus low-rank" graphical models: An optimization approach," in *2018 IEEE Conference on Decision and Control (CDC)*, pp. 2241–2246, Dec 2018.

[36] S. Talukdar, D. Deka, D. Materassi, and M. Salapaka, "Exact topology reconstruction of radial dynamical systems with applications to distribution system of the power grid," in *2017 American Control Conference (ACC)*, pp. 813–818, 2017.

[37] V. Chandrasekaran, S. Sanghavi, P. Parrilo, and A. Willsky, "Rank-sparsity incoherence for matrix decomposition," *SIAM Journal on Optimization*, vol. 21, no. 2, pp. 572–596, 2011.

[38] R. Kannan and C. L. Monma, "On the computational complexity of integer programming problems," in *Optimization and Operations Research* (R. Henn, B. Korte, and W. Oettli, eds.), (Berlin, Heidelberg), pp. 161–172, Springer Berlin Heidelberg, 1978.

[39] G. Joseph, *Linear Dynamical systems with sparsity constraints: theory and algorithms*. PhD thesis, Dept. Elect. Comm. Eng., Indian Institute of Science, Bangalore, India, 2019.

[40] M. Fazel, *Matrix Rank Minimization with Applications*. Ph. D. thesis, Department of Electrical Engineering, Stanford University, Palo Alto, CA, 2002.

[41] D. A. Cox, J. Little, and D. O'Shea, *Ideals, Varieties, and Algorithms-An Introduction to Computational Algebraic Geometry and Commutative Algebra*. Springer, 2007.

[42] K. Kozhasov, "On minimality of determinantal varieties," arXiv preprint arXiv:2003.01049.

[43] V. Mishfad S, H. Doddi, and M. V. Salapaka, "Topology learning of linear dynamical systems with latent nodes using matrix decomposition," *arXiv preprint arXiv:1912.07152*, 2019.

[44] D. Hsu, S. M. Kakade, and T. Zhang, "Robust matrix decomposition with sparse corruptions," *IEEE Transactions on Information Theory*, vol. 57, pp. 7221–7234, Nov 2011.

[45] R. A. Horn and C. R. Johnson, *Matrix Analysis*. USA: Cambridge University Press, 2nd ed., 2012.

[46] "Linearizing ODEs," 3 2021. [Online; accessed 2021-06-26].

[47] A. Goldenshluger and A. Zeevi, "Nonasymptotic bounds for autoregressive time series modeling," *Ann. Statist.*, vol. 29, pp. 417–444, 04 2001.

[48] J. Lofberg, "Yalmip : a toolbox for modeling and optimization in matlab," in *2004 IEEE International Conference on Robotics and Automation (IEEE Cat. No.04CH37508)*, pp. 284–289, Sep. 2004.

[49] M. J. T. K. C. Toh and R. H. Tutuncu, "Sdpt3—a matlab software package for semidefinite-quadratic-linear programming," in *http://www.math.nus.edu.sg/ mattohkc/sdpt3.html*.

[50] B. Lee and A. Lamperski, "Non-asymptotic closed-loop system identification using autoregressive processes and hankel model reduction," *arXiv preprint arXiv:1909.02192*, 2019.

Mishfad S. V. is a Ph.D. candidate in the Electrical and Computer Engineering Department at the University of Minnesota, Minneapolis since 2018. He received the M. E. degree in Telecommunication Engineering from the Indian Institute of Science, Bangalore, India, in 2014. His research interests include optimization, system identification, estimation theory, information theory and statistical learning.

Harish Doddi is a Ph.D. candidate in the Mechanical Engineering Department at the University of Minnesota, Minneapolis since 2016. He obtained his B.Tech degree from Indian Institute of Technology Madras, Chennai in 2014 and worked on Thermal Analysis of Commercial Buildings at the TCS Innovation Lab, Chennai, India till 2016. His research includes Information Thermodynamics, Energy limits in Computing and Structure learning of Graphical models.

Murti V. Salapaka received the B.Tech. degree in Mechanical Engineering from the Indian Institute of Technology, Madras, in 1991 and the M.S. and Ph.D. degrees in Mechanical Engineering from the University of California at Santa Barbara, in 1993 and 1997, respectively. He was a faculty member in the Electrical and Computer Engineering Department, Iowa State University, Ames, from 1997 to 2007. Currently, he is the Director of Graduate Studies and the Vincentine Hermes Luh Chair Professor in the Electrical and Computer Engineering Department, University of Minnesota, Minneapolis. His research interests include control and network science, nanoscience and single molecule physics. Dr. Salapaka received the 1997 National Science Foundation CAREER Award and is an IEEE fellow.

0018-9286 (c) 2021 IEEE. Personal use is permitted, but republication/redistribution requires IEEE permission. See http://www.ieee.org/publications_standards/publications/rights/index.html for more information.
Authorized licensed use limited to: University of Minnesota. Downloaded on August 12,2022 at 21:08:33 UTC from IEEE Xplore. Restrictions apply.